Cell Reports

Article

A selective p53 activator and anticancer agent to improve colorectal cancer therapy

Graphical abstract

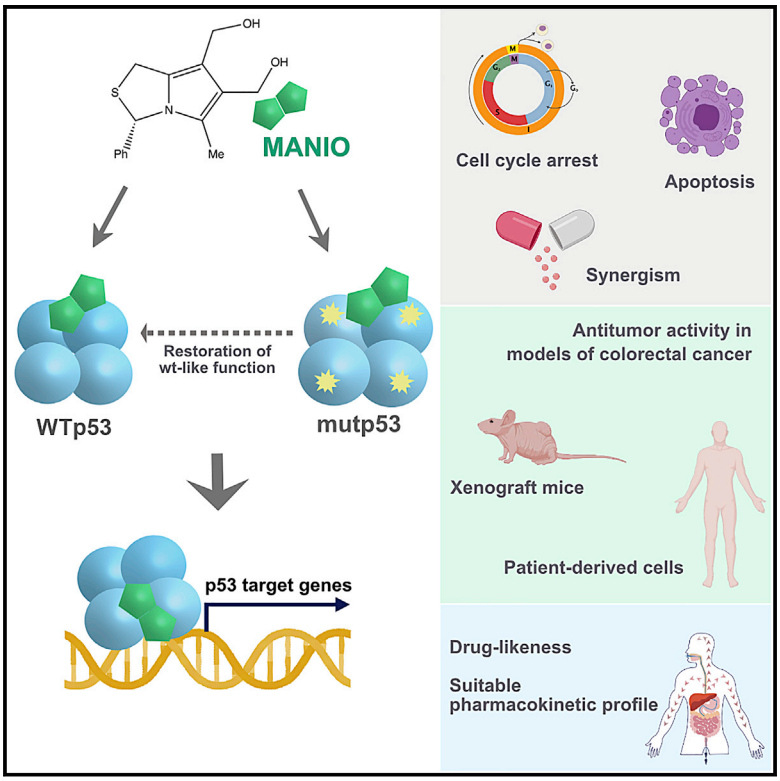

Highlights

- MANIO displays *in vitro* and *in vivo* p53-dependent antitumor activity
- MANIO activates WTp53 and restores WT-like function to mutp53 in CRC cells
- MANIO binds to WT- and mutp53 proteins, enhancing their transcriptional activity
- MANIO synergizes with conventional chemotherapeutics used in CRC therapy

Authors

Helena Ramos, Maria I.L. Soares, Joana Silva, ..., Alberto Inga, Teresa M.V.D. Pinho e Melo, Lucília Saraiva

Correspondence

tmelo@ci.uc.pt (T.M.V.D.P.e.M.), lucilia.saraiva@ff.up.pt (L.S.)

In brief

The activation of p53 is an encouraging anticancer strategy. Here, Ramos et al. present the compound MANIO, which selectively activates WTp53 and restores WT-like function to mutant p53. MANIO displays promising antitumor activity against colorectal cancer and may advance anticancer-targeted therapy, particularly benefiting colorectal cancer patients with distinct p53 status.

Ramos et al., 2021, Cell Reports *35*, 108982
April 13, 2021
https://doi.org/10.1016/j.celrep.2021.108982

CellPress

Cell Reports

CellPress
OPEN ACCESS

Article

A selective p53 activator and anticancer agent to improve colorectal cancer therapy

Helena Ramos,[1] Maria I.L. Soares,[2] Joana Silva,[3] Liliana Raimundo,[1] Juliana Calheiros,[1] Célia Gomes,[4,5,6] Flávio Reis,[4,5,6] Filipe A. Monteiro,[7,8,9] Cláudia Nunes,[10] Salette Reis,[10] Bartolomeo Bosco,[11] Silvano Piazza,[11] Lucília Domingues,[3] Petr Chlapek,[12,13] Petr Vlcek,[14] Pavel Fabian,[15] Ana Teresa Rajado,[16] A.T.P. Carvalho,[16] Renata Veselska,[12,13] Alberto Inga,[11] Teresa M.V.D. Pinho e Melo,[2,*] and Lucília Saraiva[1,17,*]

[1]LAQV/REQUIMTE, Laboratório de Microbiologia, Departamento de Ciências Biológicas, Faculdade de Farmácia, Universidade do Porto, Porto, Portugal
[2]University of Coimbra, Coimbra Chemistry Centre and Department of Chemistry, 3004-535 Coimbra, Portugal
[3]CEB-Centre of Biological Engineering, University of Minho, Campus de Gualtar, 4710-057 Braga, Portugal
[4]University of Coimbra, Coimbra Institute for Clinical and Biomedical Research (iCBR), Faculty of Medicine, Coimbra, Portugal
[5]University of Coimbra, Center for Innovative Biomedicine and Biotechnology (CIBB), Coimbra, Portugal
[6]Clinical Academic Center of Coimbra (CACC), Coimbra, Portugal
[7]Departamento de Biomedicina, Unidade de Biologia Experimental, FMUP - Faculdade de Medicina da Universidade do Porto, 4200-319 Porto, Portugal
[8]Pain Research Group, IBMC - Instituto de Biologia Celular e Molecular, 4150-180 Porto, Portugal
[9]i3S - Instituto de Investigação e Inovação em Saúde, Universidade do Porto, 4150-180 Porto, Portugal
[10]LAQV/REQUIMTE, Laboratório de Química Aplicada, Departamento de Ciências Químicas, Faculdade de Farmácia, Universidade do Porto, Porto, Portugal
[11]Department CIBIO, Laboratory of Transcriptional Networks, University of Trento, via Sommarive 9, 38123 Trento, Italy
[12]Laboratory of Tumor Biology, Department of Experimental Biology, Faculty of Science, Masaryk University, Brno, Czech Republic
[13]International Clinical Research Center, St. Anne's University Hospital, Brno, Czech Republic
[14]1st Department of Surgery, St. Anne's University Hospital, Brno, Czech Republic
[15]Department of Oncological and Experimental Pathology, Masaryk Memorial Cancer Institute, Brno, Czech Republic
[16]CNC-Center for Neuroscience and Cell Biology, University of Coimbra, 3004-504 Coimbra, Portugal
[17]Lead contact
*Correspondence: tmelo@ci.uc.pt (T.M.V.D.P.e.M.), lucilia.saraiva@ff.up.pt (L.S.)
https://doi.org/10.1016/j.celrep.2021.108982

SUMMARY

Impairment of the p53 pathway is a critical event in cancer. Therefore, reestablishing p53 activity has become one of the most appealing anticancer therapeutic strategies. Here, we disclose the p53-activating anticancer drug (3*S*)-6,7-bis(hydroxymethyl)-5-methyl-3-phenyl-1*H*,3*H*-pyrrolo[1,2-*c*]thiazole (MANIO). MANIO demonstrates a notable selectivity to the p53 pathway, activating wild-type (WT)p53 and restoring WT-like function to mutant (mut)p53 in human cancer cells. MANIO directly binds to the WT/mutp53 DNA-binding domain, enhancing the protein thermal stability, DNA-binding ability, and transcriptional activity. The high efficacy of MANIO as an anticancer agent toward cancers harboring WT/mutp53 is further demonstrated in patient-derived cells and xenograft mouse models of colorectal cancer (CRC), with no signs of undesirable side effects. MANIO synergizes with conventional chemotherapeutic drugs, and *in vitro* and *in vivo* studies predict its adequate drug-likeness and pharmacokinetic properties for a clinical candidate. As a single agent or in combination, MANIO will advance anticancer-targeted therapy, particularly benefiting CRC patients harboring distinct p53 status.

INTRODUCTION

Colorectal cancer (CRC) is currently the third most common cancer type and one of the leading causes of death worldwide (International Agency for Research on Cancer and World Health Organization, 2019). The increasing incidence of early-onset cases, due to Western diet and lifestyle, has emphasized the concern of the clinical community regarding CRC (Dekker et al., 2019; Araghi et al., 2019). Moreover, the commonly associated high mortality and therapeutic resistance have exposed the fragility of its treatment (Dekker et al., 2019). Considerable advances in pathophysiological understanding of CRC have paved the way to an array of targeted therapies for its personalized treatment. In particular, the disruption of the p53 pathway, mostly by *TP53* mutation or p53 inhibition through interaction with negative regulators, is a major pathological event in local and advanced CRC (Li et al., 2015). The tumor suppressor protein p53 is the central hub of a complex molecular network, coordinating major

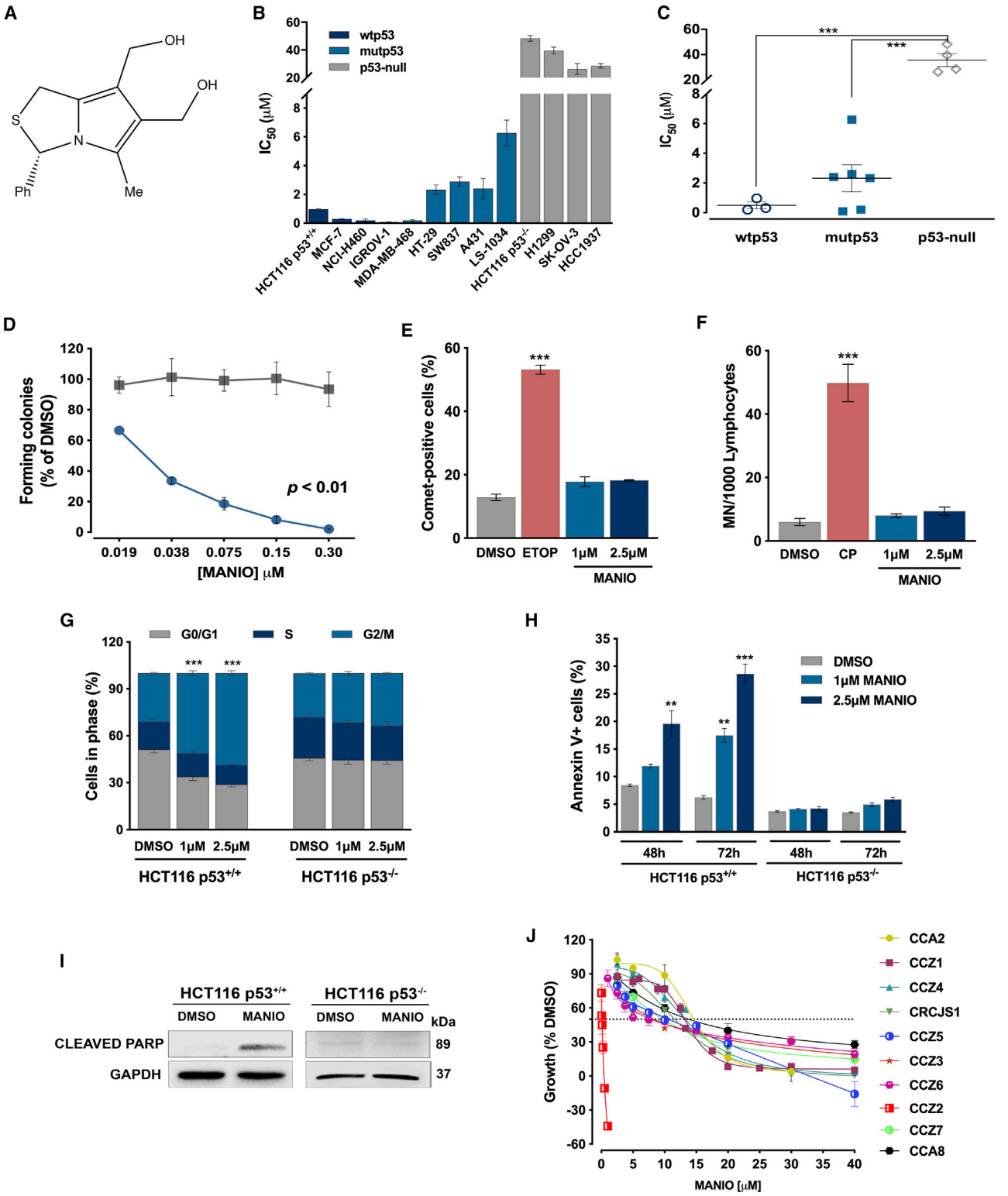

Figure 1. Growth-inhibitory effect of MANIO in human cancer cells is dependent on p53 and is associated with induction of cell-cycle arrest and apoptosis, but not genotoxicity

(A) Chemical structure of MANIO.

(legend continued on next page)

cellular responses to potentially oncogenic stimuli (Vousden and Prives, 2009). Its function relies mainly in the sequence-specific transcriptional regulation of multiple target genes mostly associated with cell cycle, apoptosis, DNA repair, and senescence (Fischer, 2017). Notably, ~80% of metastatic and advanced CRCs present *TP53* mutations that greatly contribute to its aggressiveness and invasiveness (Nakayama and Oshima, 2019). In fact, while most mutations decrease p53 DNA-binding ability and impair its transcriptional activity, specific mutant (mut) p53 proteins may also acquire additional oncogenic activities (gain of function [GOF]), contributing to worse outcomes, chemoresistance, and relapse events (Yue et al., 2017). The majority of p53 mutations are missense and are clustered in the DNA-binding domain (DBD), an essential region for p53 to recognize specific DNA sequences in the promoters of its target genes (Yue et al., 2017). Interestingly, a great proportion of mutp53 falls within six "hotspot" amino acid residues, namely R248, G245, R175, R273, R249, and R282 (Muller and Vousden, 2014; Yue et al., 2017). These mutations were categorized as contact or structural, depending on whether the residues have a role in direct DNA contact or in the maintenance of wild-type (WT)p53 conformation, respectively (Muller and Vousden, 2014; Yue et al., 2017). Specifically, substitutions at residues R175, R248, and R273 are the most frequent mutp53 in CRC (The Cancer Genome Atlas, 2012).

It is widely accepted that the restoration of p53 function is an encouraging strategy in anticancer therapy. However, although the number of p53 activators reported to date seem to be numerous, most of them have remained in the preclinical stage due to their lack of specificity (Li et al., 2019). In fact, p53-based therapy is still not clinically available for cancer treatment. Moreover, among the p53-targeting compounds under clinical trials (Merkel et al., 2017), the Nutlins (NCT03566485, NCT02633059, NCT03566485; Phases I/II) are not active on mutp53 (Kocik et al., 2019), and PRIMA-1^{MET} (APR-246; NCT03745716; Phase III) has a p53-independent inhibitory activity in CRC (Lu et al., 2016). Also, the precise mechanism of antitumor activity of the mutp53 reactivator COTI-2 (NCT02433626; Phase I) is still not comprehensively understood in many cancers, including CRC (Salim et al., 2016). Therefore, further research has been pursued to find novel p53-targeting agents that could be used as effective anticancer therapeutic options in CRC patients.

Here, the (3*S*)-6,7-bis(hydroxymethyl)-5-methyl-3-phenyl-1*H*,3*H*-pyrrolo[1,2-*c*]thiazole (MANIO) was identified as a WT- and mutp53-activating agent. MANIO directly binds to p53 DBD, displaying pronounced *in vitro* and *in vivo* antitumor activity, particularly against CRC, and exhibiting suitable drug-likeness and pharmacokinetic (PK) properties.

RESULTS

MANIO displays p53-dependent growth-inhibitory effect in human cancer cells, inducing cell-cycle arrest and apoptosis in CRC cells

In an attempt to identify new effective p53-activating agents with antitumor activity, the antiproliferative effect of a small chemical library of 6,7-bis(hydroxymethyl)-1*H*,3*H*-pyrrolo[1,2-*c*]thiazoles was investigated in a panel of human cancer cells with different p53 status. According to the half-maximal inhibitory concentration (IC_{50}) values obtained, MANIO (Figure 1A) showed noticeable selectivity to p53-expressing cancer cells. In fact, results clearly demonstrated that MANIO had a p53-dependent antiproliferative activity against cancer cells, with significantly lower IC_{50} values in cancer cells expressing WTp53 (0.20–0.97 μM) or mutp53 (0.088–6.27 μM), compared to p53 null cells (26.20–48.25 μM) (Figures 1B, 1C, and S1A). In particular, the IC_{50} value of MANIO in WTp53-expressing HCT116 colon cells (HCT116 $p53^{+/+}$; 0.97 μM) was ~50-fold lower than that obtained in the p53 null isogenic derivative (HCT116 $p53^{-/-}$; 48.25 μM) (Figures 1B and S1A). Accordingly, MANIO did not significantly affect colony formation in HCT116 $p53^{-/-}$ cells, while a pronounced

(B) IC_{50} values of MANIO in a panel of human cancer cell lines with distinct p53 status. Growth-inhibitory effect of MANIO was determined by the SRB assay, after 48 h of treatment. Growth obtained with control (DMSO) was set as 100%. Data are means ± SEMs of 4–5 independent experiments.
(C) Scatterplot representation of the relationship between MANIO IC_{50} values and p53 status in cancer cells. Data are means ± SEMs of 4–5 independent experiments; values significantly different: ***$p < 0.001$; 2-way ANOVA with Dunnett's multiple comparisons test.
(D) Effect of MANIO on colony formation of $p53^{+/+}$ and $p53^{-/-}$ HCT116 cells, after 14 days of treatment (representative images are shown in Figure S1A). Data are means ± SEMs of 4 independent experiments; $p < 0.01$; 2-way ANOVA with Sidak's multiple comparisons test.
(E) Measurement of DNA damage in HCT116 $p53^{+/+}$ cells with 1 and 2.5 μM MANIO and 25 μM etoposide (ETOP; positive control), after 48 h of treatment, using the alkaline comet assay. Quantification of comet-positive cells (containing >5% of DNA in the tail); data are means ± SEMs of 3 independent experiments (100 cells were analyzed per sample; representative images are shown in Figure S1C); 3 independent experiments; values significantly different from DMSO: ***$p < 0.001$; 1-way ANOVA with Dunnett's multiple comparisons test.
(F) Cytokinesis-block micronucleus (MN) assay after 72 h of treatment, in human lymphocyte cells; 5 μg/mL cyclophosphamide (CP): positive control; the number of MN per 1,000 binucleated lymphocytes was recorded (3 independent experiments); values significantly different from DMSO: ***$p < 0.001$; 1-way ANOVA with Dunnett's multiple comparisons test.
(G) Effect of MANIO on cell-cycle progression of $p53^{+/+}$ and $p53^{-/-}$ HCT116 cells, after 48 h of treatment. Cell-cycle phases were analyzed by flow cytometry using propidium iodide (PI), and quantified using FlowJo software. Data are means ± SEMs of 3 independent experiments; values significantly different from DMSO: ***$p < 0.001$; 2-way ANOVA with Dunnett's multiple comparisons test.
(H) Effect of MANIO on apoptosis of $p53^{+/+}$ and $p53^{-/-}$ HCT116 cells after 48 and 72 h of treatment. Apoptosis was analyzed by flow cytometry using fluorescein isothiocyanate (FITC)-annexin V and PI. Data are means ± SEMs of 3 independent experiments; values significantly different from DMSO: **$p < 0.01$; ***$p < 0.001$; 2-way ANOVA with Dunnett's multiple comparisons test.
(I) Effect of 1 μM MANIO on PARP cleavage, after 72 h of treatment, in $p53^{+/+}$ and $p53^{-/-}$ HCT116 cells. Immunoblots are representative of 3 independent experiments. Glyceraldehyde 3-phosphate dehydrogenase (GAPDH) was used as a loading control.
(J) Concentration-response curves of the growth inhibitory effect of MANIO in patient-derived CRC cells was determined by 3-(4,5-dimethylthiazol-2-yl)-2,5-diphenyltetrazolium bromide (MTT) assay, after 48 h of treatment. Data are means ± SEMs (5–8 independent experiments).

growth-inhibitory effect was observed in HCT116 $p53^{+/+}$ cells (Figures 1D and S1B).

Notably, although highly effective on CRC cells expressing WT- or mutp53 (HCT116 $p53^{+/+}$, SW837, HT-29, LS1034; IC_{50} values from 0.97 to 6.27 μM; Figure 1B), the growth-inhibitory activity of MANIO against normal CCD-18Co colon cells (IC_{50} of 32.83 ± 1.69 μM, n = 5) was much lower, which demonstrated its selectivity to cancer cells.

We next checked whether the antiproliferative effect of MANIO was associated with the induction of DNA damage. For that, the potential genotoxicity of MANIO was assessed in cancer and normal cells by comet assay and micronucleus (MN) test, respectively. Contrary to the positive controls, 1 and 2.5 μM MANIO did not increase the percentage of comet-positive HCT116 $p53^{+/+}$ cells (Figures 1E and S1C) and the number of formed micronuclei in peripheral lymphocytes of normal individuals (Figure 1F). However, 1 and 2.5 μM MANIO induced G2/M phase cell-cycle arrest (Figure 1G) and increased the percentage of annexin V^+ cells (Figure 1H) in $p53^{+/+}$, but not in $p53^{-/-}$, HCT116 cells. The stimulation of a p53-dependent apoptotic cell death by MANIO was further evidenced by the induction of poly-ADP ribose polymerase (PARP) cleavage, at 1 μM, in $p53^{+/+}$, but not in $p53^{-/-}$, HCT116 cells (Figure 1I).

The growth-inhibitory effect of MANIO was further checked in a panel of patient-derived primary CRC cells, as a more disease-relevant model system, closer to the heterogeneity and intrinsic drug sensitivity of the original tumors (Jabs et al., 2017). All CRC cells expressed WTp53, except for CCA8, which harbored mutp53 P151S (Table S1). MANIO inhibited the growth of all patient-derived CRC cells with similar IC_{50} values ranging from 9.46 to 15.43 μM (Figure 1J; Table S1). The only exception occurred with the CCZ2 cells (IC_{50} value of 0.09 μM), which were already subjected to a previous therapy. In fact, CCZ2 cells derived from a patient diagnosed with liver metastatic adenocarcinoma that was first subjected to 5-fluorouracil (5-FU) and oxaliplatin plus the anti-angiogenic agent bevacizumab (Table S1), following by surgical removal of the remaining liver metastasis.

MANIO activates the p53 pathway in CRC cells by binding to p53 DBD, with induction of p53 stabilization and enhancement of its DNA-binding ability and transcriptional activity

To gain additional evidence of the potential of MANIO to engage the p53 response pathway, WTp53-expressing HCT116-treated cells were analyzed by RNA sequencing (RNA-seq). MANIO treatment led to broad changes in gene expression, with nearly 900 upregulated and 500 downregulated differentially expressed genes (DEGs) (data are deposited in GEO: GSE145482; Figures 2A and 2B). Gene Ontology, pathway, and upstream regulator enrichment analysis using the EnrichR web tool (Kuleshov et al., 2016) strongly evidenced an activation of the p53-response pathway (Figures 2C and 2D). Instead, the list of genes repressed by MANIO diverged from a canonical p53-dependent signature, as it was not enriched for cell proliferation, DNA repair, DNA replication, or cell division (Figures 2C and 2E). Similar results were obtained using gene set enrichment analysis (GSEA) (data not shown) or Metascape (Figures S2A and S2B). Approximately 65 established p53 target genes were upregulated by MANIO in the RNA-seq data (Figure 2D). Hence, the upregulated gene signature of MANIO-treated HCT116 cells is indisputably p53-related. p53-dependent gene repression is thought to be mostly indirect and largely dependent on the modulation of the DREAM (dimerization partner, RB-like, E2F, and multi-vulval class B) complex via p21 (Engeland, 2018), which is induced by MANIO. Hence, we compared MANIO downregulated DEGs with an extended list of DREAM complex targets and found a very small overlap (Figure S2C). However, a trend for downregulation by MANIO of several DREAM targets was observed (Figure S2D). We then explored whether the lack of a canonical p53-dependent gene repression signature could be dependent on the time point of the RNA-seq by following 4 DREAM targets in MANIO-treated cells for 16, 24, and 48 h (Figure S2E). Results confirmed the RNA-seq data and also showed the same trend for the earlier time point, while the 48-h treatment showed a trend for downregulation, paralleled by the higher induction of p21. The results therefore indicated that MANIO engaged the p53-dependent response, with its effects persisting and increasing over at least a 48-h time window.

Consistently, in HCT116 $p53^{+/+}$ cells, MANIO treatment increased p53 protein levels in a dose- and time-dependent manner (Figures 3A and 3B), which was related to p53 stabilization (Figures 3C and 3D). In fact, an enhancement of p53 half-life by MANIO was observed upon the inhibition of protein synthesis with cycloheximide (CHX). Moreover, MANIO regulated the protein levels of major p53 transcriptional targets, increasing MDM2, p21, GADD45, PUMA, and Killer/DR5, while decreasing the anti-apoptotic BCL-2 in $p53^{+/+}$, but not in $p53^{-/-}$, HCT116 cells (Figures 3E and 3F). Accordingly, MANIO upregulated the mRNA levels of the p53 transcriptional targets *MDM2*, *CDKN1A/p21*, *GADD45A*, *BAX*, *TNFRSF10B/DR5*, *PUMA*, and *NOXA* in HCT116 $p53^{+/+}$ cells (Figure 3G) without affecting their expression in HCT116 $p53^{-/-}$ cells (Figure 3H).

Similarly, in WTp53-expressing patient-derived CCZ1, CCZ2, CCZ3, and CCZ5 cells, MANIO engaged a p53 response by interfering with mRNA expression levels of several p53 transcriptional targets, increasing *BAX*, *CDKN1A/p21*, and *MDM2* (Figures 3I–3L), while decreasing the levels of the angiogenic factor *VEGF* in CCZ1, CCZ3, and CCZ5 (Figures 3I, 3J, and 3L). Importantly, in CCZ1, CCZ2, and CCZ3 cells, MANIO also significantly decreased the mRNA expression levels of the pro-survival *BIRC5* (Figures 3I–3K), which is a critical gene in cancer cell growth and chemoresistance.

Via the chromatin immunoprecipitation (ChIP) assay, we could verify that the increase of p53 transcriptional activity by MANIO resulted from an enhancement of p53 DNA-binding ability in HCT116 $p53^{+/+}$ cells. In fact, MANIO increased the p53 occupancy at the *MDM2* and *CDKN1A* promoters (Figure 3M).

For an in-depth understanding of the mode of action of MANIO, we started by checking the potential binding of MANIO to WTp53 by cellular thermal shift assay (CETSA) analysis. The results showed that 30 μM MANIO induced WTp53 thermal stability at 38°C and 39°C (Figure 3N), causing a concentration-dependent WTp53 thermal stability at 39°C, when compared to solvent (Figures 3O and 3P), in HCT116 $p53^{+/+}$ cells. In CETSA, upon gradual heating, unbound proteins denature and precipitate, while a small-molecule ligand can counteract this effect by providing thermodynamic stability to a target protein,

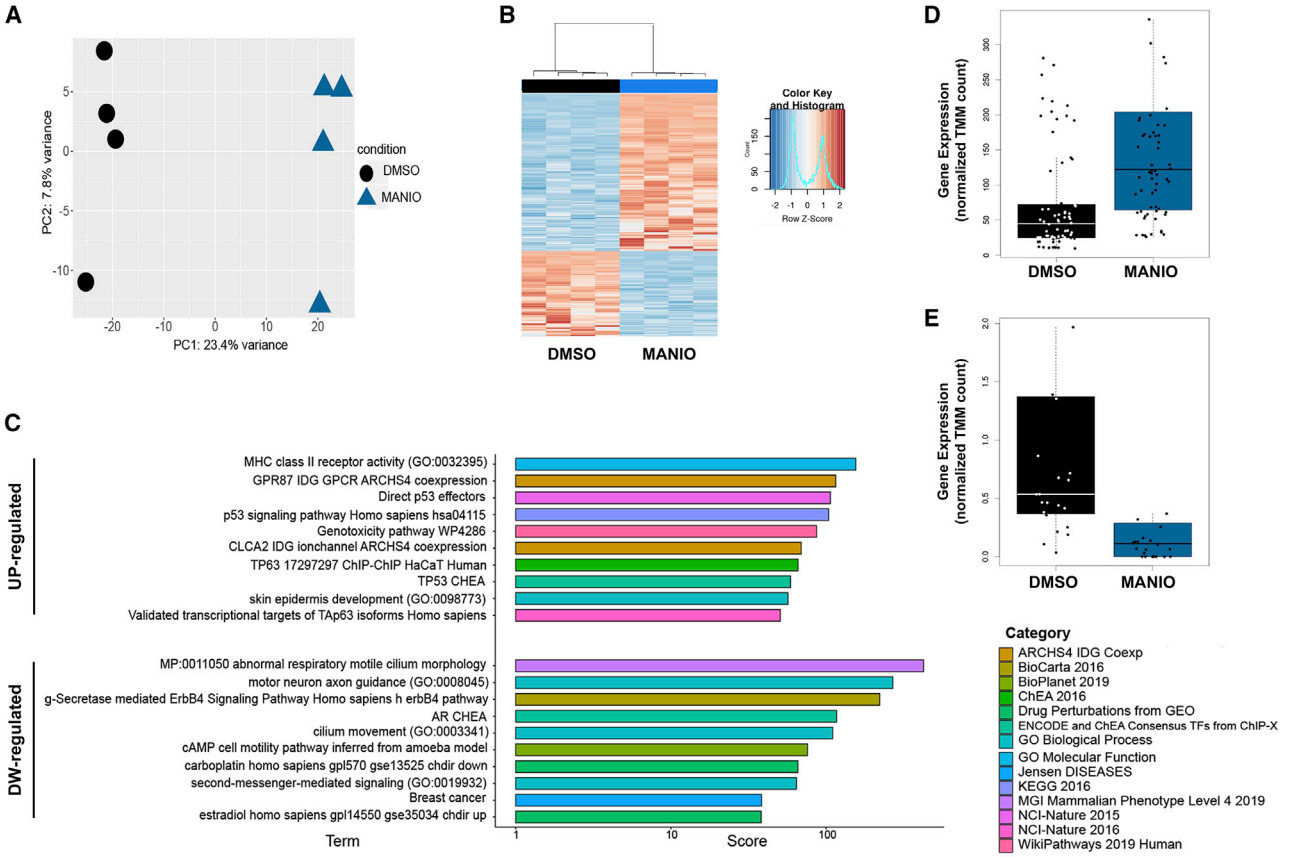

Figure 2. Gene expression profile changes in human cancer cells by MANIO reveal a p53-activating signature

(A) Principal-component analysis (PCA) (Fernandes et al., 2017) of the gene expression counts (log2 normalized trimmed mean of M values [TMM] method counts) showing the first versus the second PC. In the axes, the percentage of the explained variance by the component is reported. Samples in the 2 conditions (DMSO, 1 μM MANIO) are highlighted in different colors and different shapes.

(B) Heatmap showing the differentially expressed genes (log2 fold change <−1 or >1, multiple tests correction, adjusted $p < 0.05$) in the comparison of MANIO versus DMSO. Gene expression counts were normalized by the TMM method, hierarchically clustered with average linkage, and uncentered correlation metric was applied. Two main clusters of genes were obtained: the first comprises the genes upregulated through the samples cluster and a second one comprises the genes downregulated.

(C) Bar plot graphs represent the enrichment of the biological terms based on the combined score (x axis), as calculated by the EnrichR web tool; upper panel: upregulated (UP) gene cluster, bottom panel: downregulated (DW) gene cluster. Since this tool provides a large collection of gene set databases, a few key elements were selected for each (full results in Figure S2). All of the terms have multiple test correction adjusted $p < 0.05$.

(D and E) Boxplot representations of the RNA-seq-based gene expression for 1 element from the upregulated gene cluster (p53 signaling pathway (D) and 1 element from the downregulated gene cluster (cyclic AMP [cAMP]-mediated cell motility pathway genes (E).

subsequently increasing its fraction in solution (Martinez Molina and Nordlund, 2016). Based on this premise, the increase in the amount of soluble WTp53, after the heating of cell lysates, indicated potential protein-ligand interactions. To confirm these results evidenced by CETSA, the human WTp53 DBD was produced in *Escherichia coli* for a binding fluorescence quenching assay. The binding assay confirmed that MANIO directly bound to WTp53 DBD (K_d of 590 ± 90 μM; Figure 3Q).

MANIO synergizes with conventional chemotherapeutics in patient-derived CRC cells expressing WTp53

The ability of MANIO to enhance the anticancer activity of conventional chemotherapeutic drugs, including doxorubicin (DOXO) and cisplatin (CISP), was investigated in patient-derived CCZ3 cells expressing WTp53. Platinum-based agents (CISP) are typically included in the first-line regimens for CRC treatment (Yau, 2019). DOXO has limited efficacy against CRC due to frequent multidrug resistance (Khaleel et al., 2016). CCZ3 cells were treated with a range of concentrations of DOXO or CISP alone and in combination with 2 μM MANIO followed by the determination of cell proliferation, after 48 h of treatment. In combination regimes with DOXO and CISP, MANIO significantly increased the growth-inhibitory effect of these chemotherapeutic agents (Figures S3A and S3B). Consistently, synergic effects (combination index [CI] < 1) were obtained for the different combinations between MANIO and DOXO or CISP, in CCZ3 cells (Table 1). Moreover, the dose reduction index (DRI) values indicated that MANIO can reduce the effective dose of the chemotherapeutic agents

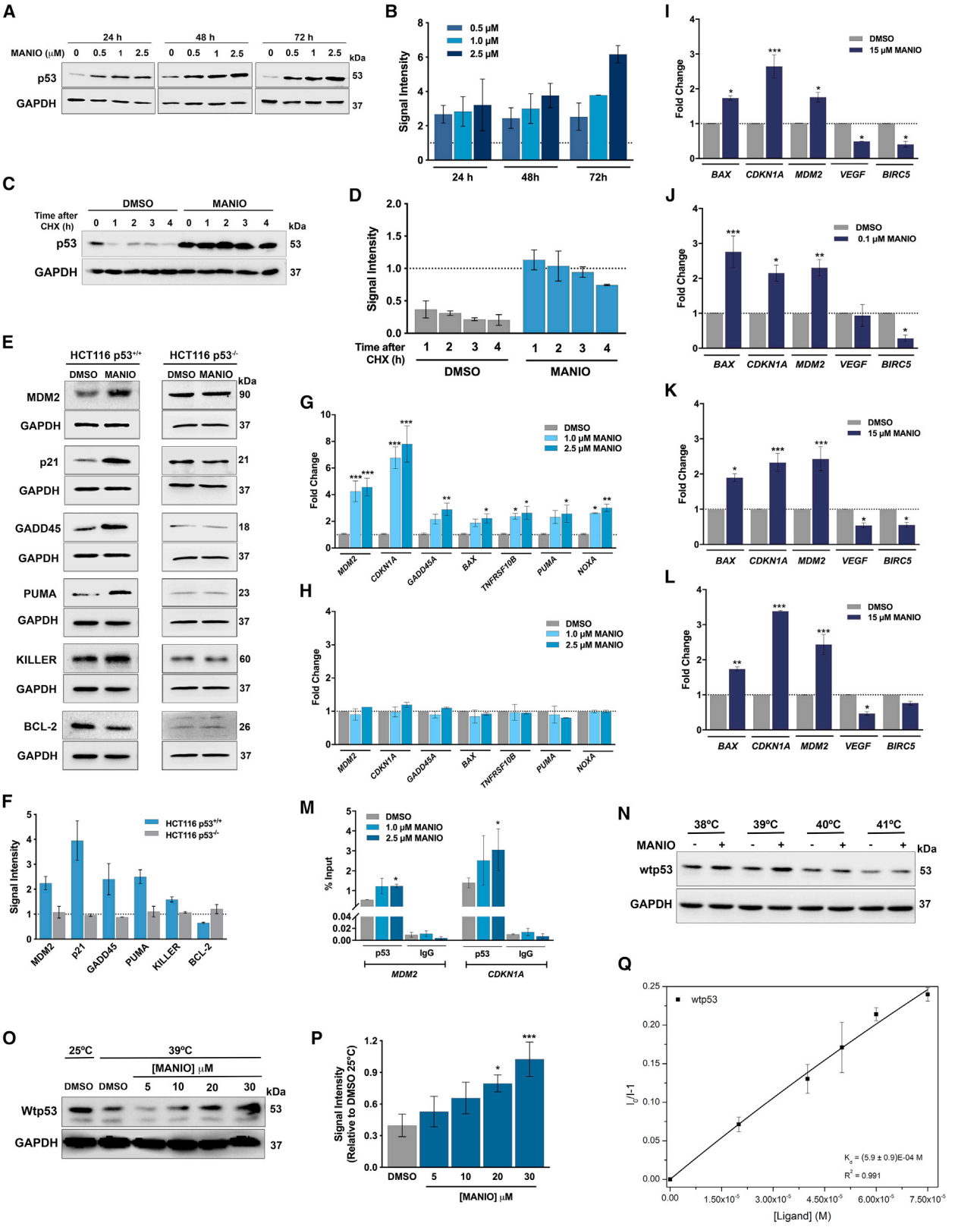

(legend on next page)

(Table 1), therefore minimizing their undesirable toxicity and commonly associated chemoresistance (Li et al., 2017).

MANIO restores WT-like properties to mutp53 R248W by directly binding to protein DBD

Given the prominent antiproliferative activity of MANIO in human cancer cells expressing distinct mutp53 forms, particularly of CRC (Figure 1B), its capacity to reactivate different structural and contact mutp53s, with high prevalence and clinical relevance in human cancers (Muller and Vousden, 2014), was further investigated. For that, these mutp53s were ectopically expressed in p53 null H1299 cancer cells, and the antiproliferative effect of MANIO was evaluated (Figure 4A). Importantly, no significant differences were detected between the protein expression levels of the different mutp53s (Figure 4A, lower panel). When compared to cells transfected with the empty vector, MANIO showed a significant reduction of its IC_{50} value in H1299 cells expressing mutp53 R282W, R248W, R280K, R273H, R273C, G245D, R175H, R248Q, or G245S (Figure 4A). Despite the large panel of mutp53 potentially reactivated by MANIO, its highest inhibitory effect was achieved on cells expressing mutp53 R248W or R248Q, while no reduction in IC_{50} was observed for mutp53 Y220C, which suggested some level of selectivity for mutp53 forms. Importantly, the high IC_{50} values of MANIO in both parental (39.50 ± 2.50 μM; Figure 1B) and empty vector-transfected (41.25 ± 1.61 μM; Figure 4A) H1299 cancer cells further reinforced its mutp53-dependent antiproliferative activity.

To gain a deeper understanding of the ability of MANIO to reactivate mutp53, we focused on mutp53 R248W. The prominent growth-inhibitory effect displayed by MANIO in SW837 rectum cells, which endogenously express mutp53 R248W, by sulforhodamine (SRB) assay (IC_{50} of 2.9 ± 0.32 μM; Figure 1B), was also confirmed by colony-formation assay (Figures 4B and S4A). Furthermore, MANIO induced apoptotic cell death in SW837 cells (Figure 4C). Consistently with a reactivation of mutp53 R248W, MANIO increased the protein levels of p53 transcriptional targets, including MDM2 and PUMA, an effect abolished by p53 small interfering RNA (siRNA) (Figures 4D and 4E, and S4B). Moreover, the mRNA levels of *MDM2*, *CDKN1A/p21*, and *NOXA* were upregulated in a dose-dependent manner (Figure 4F). In addition, MANIO enhanced mutp53 R248W occupancy at *MDM2* and *CDKN1A* promoters, demonstrating the restoration of mutp53 DNA-binding ability (Figure 4G).

As with WTp53, the impact of MANIO on the thermal stability of mutp53 R248W was also checked in whole and lysate SW837 cells. In cell lysates, the CETSA analysis demonstrated that MANIO induced mutp53 R248W thermal stability between 39°C and 41°C (Figure 4H). Moreover, at 40°C, MANIO caused concentration-dependent mutp53 R248W thermal stability when compared to solvent (Figures 4I and 4J). In fact, 0.75 μM MANIO promoted a complete protein stabilization, with reestablishment of the non-denatured mutp53 protein levels observed with solvent at 25°C. Consistently, in whole SW837 cells, a significant thermal stabilization of mutp53 R248W could also be observed at 40°C for 3 μM MANIO (Figures 4K and 4L). Importantly, the ability of MANIO to induce the thermal stability of other mutp53, including Y126C and R273H, was also verified (Figures S4C–S4F). These results indicated a potential interaction between MANIO and mutp53. To corroborate these findings, the recombinant human mutp53 R248W DBD was produced in *Escherichia coli* and was used in a binding fluorescence quenching assay, which confirmed the direct interaction of MANIO with mutp53 R248W DBD (K_d of 320 ± 90 μM; Figure 4M).

Figure 3. MANIO directly binds to WTp53 DBD, enhancing its stabilization, DNA-binding ability, and transcriptional activity in CRC cells

(A and B) Effect of MANIO on the protein expression levels of p53, after 24, 48, and 72 h of treatment, in HCT116 $p53^{+/+}$ cells (A). (B) Quantification of p53 protein levels relative to DMSO (set as 1); data are means ± SEMs of 3 independent experiments.

(C and D) p53 protein levels in HCT116 $p53^{+/+}$ cells treated with 1 μM MANIO or solvent for 48 h followed with 150 μg/mL cycloheximide (CHX). (D) Quantification of p53 protein levels relative to 0 h (no CHX treatment) was set as 1; data are means ± SEMs of 3 independent experiments.

(E and F) Effect of 1 μM MANIO on the protein expression levels of p53 transcriptional targets, after 48 h (MDM2, p21, and GADD45) and 72 h (BCL-2, KILLER, and PUMA) of treatment, in $p53^{+/+}$ and $p53^{-/-}$ HCT116 cells. Blots of PUMA, KILLER and BCL-2 (HCT $p53^{+/+}$), p21 and GADD45 (HCT $p53^{+/+}$), MDM2 and GADD45 (HCT $p53^{-/-}$), and PUMA, KILLER and BCL-2 (HCT $p53^{-/-}$), share the same loading control GAPDH. (F) Quantification of protein expression levels in $p53^{+/+}$ and $p53^{-/-}$ HCT116 cells, relative to DMSO (set as 1); data are means ± SEMs of 3 independent experiments.

(G and H) Effect of MANIO in mRNA expression levels of p53 target genes in $p53^{+/+}$ (G) and $p53^{-/-}$ (H) HCT116 cells, after 48 h of treatment, determined by qRT-PCR. Fold of induction relative to DMSO. *GAPDH* and *B2M* were used as reference genes. Data are means ± SEMs of 3 independent experiments; values significantly different from DMSO: *$p < 0.05$; **$p < 0.01$; ***$p < 0.001$; 2-way ANOVA with Dunnett's multiple comparison test.

(I–L) Effect of MANIO in mRNA expression levels of p53 target genes in CCZ1 (I), CCZ2 (J), CCZ3 (K), and CCZ5 (L) cells, after 48 h of treatment, determined by qRT-PCR. Fold of induction is relative to DMSO. *HSP90AB1* was used as reference gene. Data are means ± SEMs of 3 independent experiments; values significantly different from DMSO: *$p < 0.05$; **$p < 0.01$; ***$p < 0.001$; unpaired Student's t test.

(M) Analysis of p53 occupancy at *MDM2* and *CDKN1A* promoters, in HCT116 $p53^{+/+}$ cells, determined by ChIP, after 48 h of treatment with 1 and 2.5 μM MANIO. Immunoprecipitation was performed using the anti-p53 antibody or an anti-mouse immunoglobulin G (IgG) as a negative control (IgG). The enrichment of DNA fragments was analyzed by qPCR using site-specific primers. Data are means ± SEMs of 3 independent experiments; values significantly different from DMSO: *$p < 0.05$; 2-way ANOVA with Dunnett's multiple comparison test.

(N–P) CETSA experiments were performed in HCT116 $p53^{+/+}$ lysates.

(N) Lysate samples, treated with DMSO (–) or MANIO (+; 30 μM), were heated at different temperatures.

(O) Lysate samples were treated with increasing concentrations of MANIO and heated at 39°C.

(P) Plotted data represent the amount of non-denatured p53 after heating in MANIO-treated lysates relative to DMSO (3 independent experiments); fold increase was calculated setting the amount of non-denatured mutp53 obtained with DMSO at 25°C as 1. Data are means ± SEMs (3 independent experiments); values significantly different from DMSO: *$p < 0.05$; ***$p < 0.001$; 2-way ANOVA with Dunnett's multiple comparisons test.

(Q) Binding of MANIO to WTp53 measured by fluorescence quenching of 5 μM WTp53 DBD recombinant protein upon MANIO titration. The K_d for the interaction was determined via nonlinear regression using the equation described in Method details.

In (A), (C), (E), (N), and (O), immunoblots are representative of 3 independent experiments; GAPDH was used as loading control.

Table 1. Effect of MANIO in combination with conventional chemotherapeutic agents, in WT- and mutp53-expressing CRC cells

Drug combination with MANIO	Mutually nonexclusive CI	DRI of conventional drug
Patient-derived CCZ3 cells		
Cisplatin (μM)		
4.9	0.75	1.33
7.4	0.81	1.23
DOXO (μM)		
0.39	0.52	2.63
0.59	0.54	2.70
0.89	0.59	2.87
1.33	0.61	1.63
SW837 cells		
DOXO (nM)		
31.25	0.38	8.19
62.5	0.34	6.35
125	0.39	4.14
250	0.51	2.60
500	0.32	3.58
5- FU (μM)		
1.25	0.31	36.52
2.5	0.26	33.97
5	0.25	22.51
10	0.25	15.15
20	0.25	11.31
Cisplatin (μM)		
2.5	0.63	9.31
5	0.68	5.36
10	0.70	3.85
20	0.37	8.84

The synergistic effect of 2 μM (CCZ3 cells) or 0.9 μM (SW837 cells) MANIO in combination with doxorubicin (DOXO), 5-fluorouracil (5-FU), or cisplatin was evaluated using CompuSyn software to calculate combination index (CI) and conventional chemotherapeutic dose reduction index (DRI) values. CI < 1, synergy. Data were calculated using a mean value effect (6 independent experiments). CRC, colorectal cancer; MANIO, (3*S*)-6,7-bis(hydroxymethyl)-5-methyl-3-phenyl-1*H*,3*H*-pyrrolo[1,2-*c*]thiazole.

MANIO synergizes with conventional chemotherapeutics in CRC cells expressing mutp53

We also analyzed the ability of MANIO to improve the anticancer activity of the conventional chemotherapeutics DOXO, 5-FU, and CISP in mutp53-expressing CRC cells. For that, SW837 cells were treated with a range of concentrations of DOXO, 5-FU, or CISP, alone and in combination with 0.9-μM MANIO, followed by evaluation of cell proliferation, after 24 h treatment. The results showed that MANIO significantly increased DOXO, CISP, and 5-FU growth-inhibitory effects (Figures S3C–S5E). Consistently, synergic effects (CI < 1) were obtained for the different combinations between MANIO and DOXO, CISP, and 5-FU, in SW837 cells (Table 1). According to DRI values, MANIO can reduce the effective dose of chemotherapeutic agents, and subsequently their undesirable toxicity and chemoresistance.

MANIO has *in vivo* p53-dependent antitumor activity in xenograft mouse models of CRC, with no apparent toxic side effects

The *in vivo* antitumor activity of MANIO was assessed using xenograft mouse models of HCT116 $p53^{+/+}$, HCT116 $p53^{-/-}$, and SW837 CRC cells. Four intraperitoneal administrations of MANIO inhibited the growth of WTp53-expressing HCT116 (100 mg/kg; Figures 5A and 5B) and mutp53-expressing SW837 (50 and 100 mg/kg; Figures 5D and 5E) tumors when compared to vehicle. Conversely, for the same conditions, MANIO did not interfere with the growth of p53 null HCT116 tumors (Figures 5G and 5H), supporting its *in vivo* p53-dependent antitumor activity.

During the experimental time, no significant loss of body weight or morbidity signs were observed in mice treated with MANIO (Figures 5C, 5F, and 5I). We also examined potential primary toxicity signs in mice induced by MANIO treatments. At the time of sacrifice, organs' relative weight and biochemical and hematological blood parameters were determined (Table S2). No significant differences regarding the weight of heart, spleen, liver, or kidneys, as well as hematological and biochemical parameters, were observed between MANIO and vehicle groups.

Tumor sections were subsequently analyzed by immunohistochemistry staining (Figures 5J–5N). In both HCT116 $p53^{+/+}$ and SW837 tumors, MANIO reduced proliferation, as demonstrated by decreased $Ki67^{+}$ staining (Figures 5J and 5K), and induced apoptosis, as demonstrated by increased Bax expression (Figures 5J and 5L) and DNA fragmentation ($TUNEL^{+}$ staining; Figures 5J and 5M) when compared to vehicle. Accordingly, no significant differences were observed in these markers between MANIO- and vehicle-treated HCT116 $p53^{-/-}$ tumors (Figures 5J–5M). Alterations in p53 expression levels were also detected in the different experimental groups. As expected, p53 expression was not observed in MANIO- or vehicle-treated HCT116 $p53^{-/-}$ tumors (Figure 5J). Also, much higher p53 levels were found in mutp53-expressing SW837 tumors than in WTp53-expressing HCT116 tumors (vehicle-treated tumors; Figures 5J and 5N). Moreover, in HCT116 $p53^{+/+}$ tumors, consistent with a p53 stabilization, MANIO increased WTp53 expression levels compared to the vehicle (Figures 5J and 5N). Conversely, in SW837 tumors, MANIO significantly decreased mutp53 expression levels (Figures 5J and 5N).

MANIO exhibits suitable drug-likeness and pharmacokinetic properties for a clinical candidate

According to solubility determinations, MANIO presented good solubility in aqueous solvents of neutral and basic pH, but not in low pH aqueous solvents (Table S3). MANIO also displayed the coefficient partition (logD) of 1.09, indicating an adequate lipophilicity and therefore its suitability to cross cellular membranes. In fact, MANIO complies all of the "rule of 5" parameters for good oral absorption, including <5 hydrogen bond donors (expressed as the sum of OHs and NHs), a molecular weight

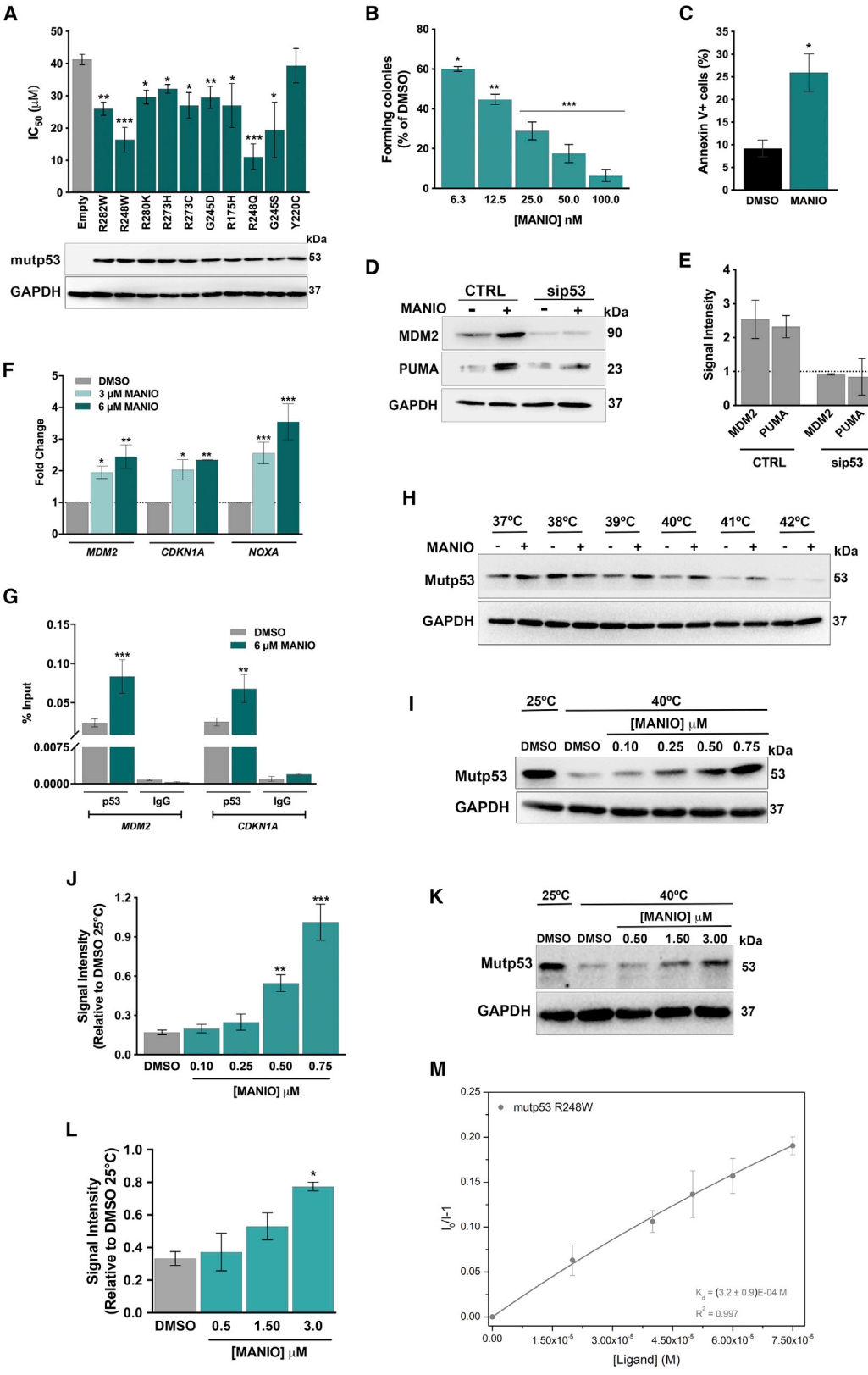

(legend on next page)

inferior to 500, a logP <5, and <10 hydrogen bond acceptors (expressed as the sum of Ns and Os) (Lipinski et al., 2001).

The study of the transport of MANIO across a Caco-2 cell monolayer to predict human intestinal permeability revealed that despite the good permeability, with a high percentage of MANIO recovery, some level of MANIO efflux was occurring (Table S4), which may limit drug absorption in the intestine.

Regarding the susceptibility of MANIO to undergo hepatic first-pass metabolism, *in vitro* models of hepatic clearance using human liver microsomes showed that MANIO exhibited relatively low intrinsic clearance (CL_{int} < 115.5 μg/min/pmol; Table S5), which may predict a slower clearance *in vivo*, and therefore a longer activity. Also, contrary to most drugs that largely bind to plasma proteins, such as albumin (Undevia et al., 2005), a negligible fraction of MANIO bound to plasmatic albumin was detected (Table S6), indicating that a high percentage of MANIO is pharmacologically active and free to distribute.

The kinetics of MANIO were also analyzed in mice treated via intravenous bolus injection, which constitutes the most direct route of administration, resulting in fast and full compound bioavailability. Given the very low fraction of protein-bound MANIO (Table S6), with free compound at ~99.6%, mice plasma level determinations were expected to represent almost all MANIO free fraction available at a given time point. The curve of total plasma concentration of MANIO versus time (Figure S5; Table S7) indicated an apparent volume of distribution at steady state (Vss) of 4 L/kg, which can be attributed to the fast body distribution of MANIO. In fact, drugs that slightly bind to plasma proteins or with good lipophilicity, such as MANIO, present high Vss (Toutain and Bousquet-Mélou, 2004). MANIO showed high clearance (CL = 26 mL/min/kg; Table S7) and an elimination half-life ($t_{1/2}$) of ~6.83 h (Table S7). Collectively, these results predict adequate drug-likeness and PK properties for MANIO.

DISCUSSION

An in-depth knowledge of CRC pathogenesis has greatly improved patient stratification, based on molecular subtypes of CRC, and therefore the personalized therapy of this type of cancer. In particular, the inactivation of the p53 pathway is an indisputable event in CRC development, which has rendered its functional restoration an appealing strategy in targeted anticancer therapy.

Here, we report the identification of the p53-activating agent MANIO, which is able to activate WTp53 and restore WT-like function to mutp53. In fact, MANIO displayed an evident p53-dependent antitumor activity, with a much higher growth-inhibitory effect on WT-/mutp53-expressing cancer cells than on p53 null cells. In particular, in WTp53-expressing CRC cells, MANIO induced cell-cycle arrest and apoptosis. Consistently, it interfered with the protein and mRNA expression levels of major p53 transcriptional targets, increasing the cell-cycle regulators p21 and GADD45 and the pro-apoptotic PUMA and KILLER/DR5, while decreasing the anti-apoptotic regulator BCL-2. These effects were associated with a marked induction of WTp53 stabilization by MANIO. Notably, we also uncovered that MANIO directly bound to the WTp53 DBD, leading to its thermal stability.

A pronounced growth-inhibitory effect of MANIO was also unveiled in cancer cells expressing distinct contact and structural

Figure 4. MANIO restores WT-like properties to mutp53: direct interaction with mutp53 R248W DBD with induction of protein thermal stability and enhancement of its DNA-binding ability and transcriptional activity

(A) p53 null H1299 cells were transfected with pcDNA3 plasmid (empty or expressing mutp53). Growth-inhibitory effect of 3.125–50 μM MANIO was determined by SRB assay after 48 h of treatment of H1299 cells. Data are means ± SEMs of 4–8 independent experiments; values significantly different from empty vector: *p < 0.05; **p < 0.01; ***p < 0.001; unpaired Student's t test. Immunoblots represent the protein expression levels of mutp53 in untreated H1299-transfected cells after 72 h of incubation.

(B) Effect of MANIO on SW837 cell colony formation after 11 days of treatment (representative images are shown in Figure S4A). Data are means ± SEMs of 4 independent experiments; values significantly different from empty vector: *p < 0.05 **p < 0.01; ***p < 0.001; 1-way ANOVA with Dunnett's multiple comparisons test.

(C) Effect of 3 μM MANIO on apoptosis of SW837 cells, after 48 h of treatment. Apoptosis was analyzed by flow cytometry using FITC-annexin V and PI. Data are means ± SEMs of 3 independent experiments; values significantly different from DMSO: *p < 0.05; unpaired Student's t test.

(D and E) Protein levels of MDM2 and PUMA, after 24 h of treatment with 3 μM MANIO, in mutp53 R248W-silenced (sip53) and control (CTRL) SW837 cells (silencing efficacy of mutp53 by siRNA is shown in Figure S4B).

(E) Quantification of protein expression levels is relative to DMSO (set as 1).

(F) Effect of MANIO on the mRNA expression levels of p53 target genes in SW837 cells after 24 h of treatment, determined by qRT-PCR. Fold of induction is relative to DMSO. *GAPDH* and *B2M* were used as reference genes. Data are means ± SEMs of 3 independent experiments; values significantly different from DMSO: *p < 0.05; **p < 0.01; ***p < 0.001; 2-way ANOVA with Dunnett's multiple comparisons test.

(G) Analysis of the p53 occupancy at *MDM2* and *CDKN1A* promoters in SW837 cells, after 24 h of treatment with MANIO, determined by ChIP. Immunoprecipitation was performed with the anti-p53 antibody or an anti-mouse IgG as a negative control (IgG). The enrichment of DNA fragments was analyzed by qPCR, using site-specific primers. Data are means ± SEMs (3 independent experiments); values significantly different from DMSO: **p < 0.01; ***p < 0.001; 2-way ANOVA with Dunnett's multiple comparisons test.

(H–L) CETSA experiments were performed in lysate (H–J) and whole (K and L) SW837 cells.

(H) Lysate samples, treated with DMSO (–) or MANIO (+; 0.75 μM), were heated at different temperatures.

(I)–(L) Samples were treated with increasing concentrations of MANIO and heated at 40°C. (J and L) Plotted data represent the amount of non-denatured p53 after heating, in MANIO-treated relative to DMSO (3 independent experiments); fold increase was calculated, setting the amount of non-denatured mutp53 obtained with DMSO at 25°C at 1. Data are means ± SEMs (3 independent experiments); values significantly different from DMSO: *p < 0.05; **p < 0.01; ***p < 0.001; 2-way ANOVA with Dunnett's multiple comparisons test.

(M) Direct binding of MANIO to mutp53 R248W DBD measured by fluorescence quenching of 5 μM mutp53 R248W recombinant protein upon MANIO titration. K_d values for the interactions were determined via nonlinear regression using the equation described in Method details.

In (A), (D), (H), (I), and (K), immunoblots are representative of 3 independent experiments; GAPDH was used as a loading control.

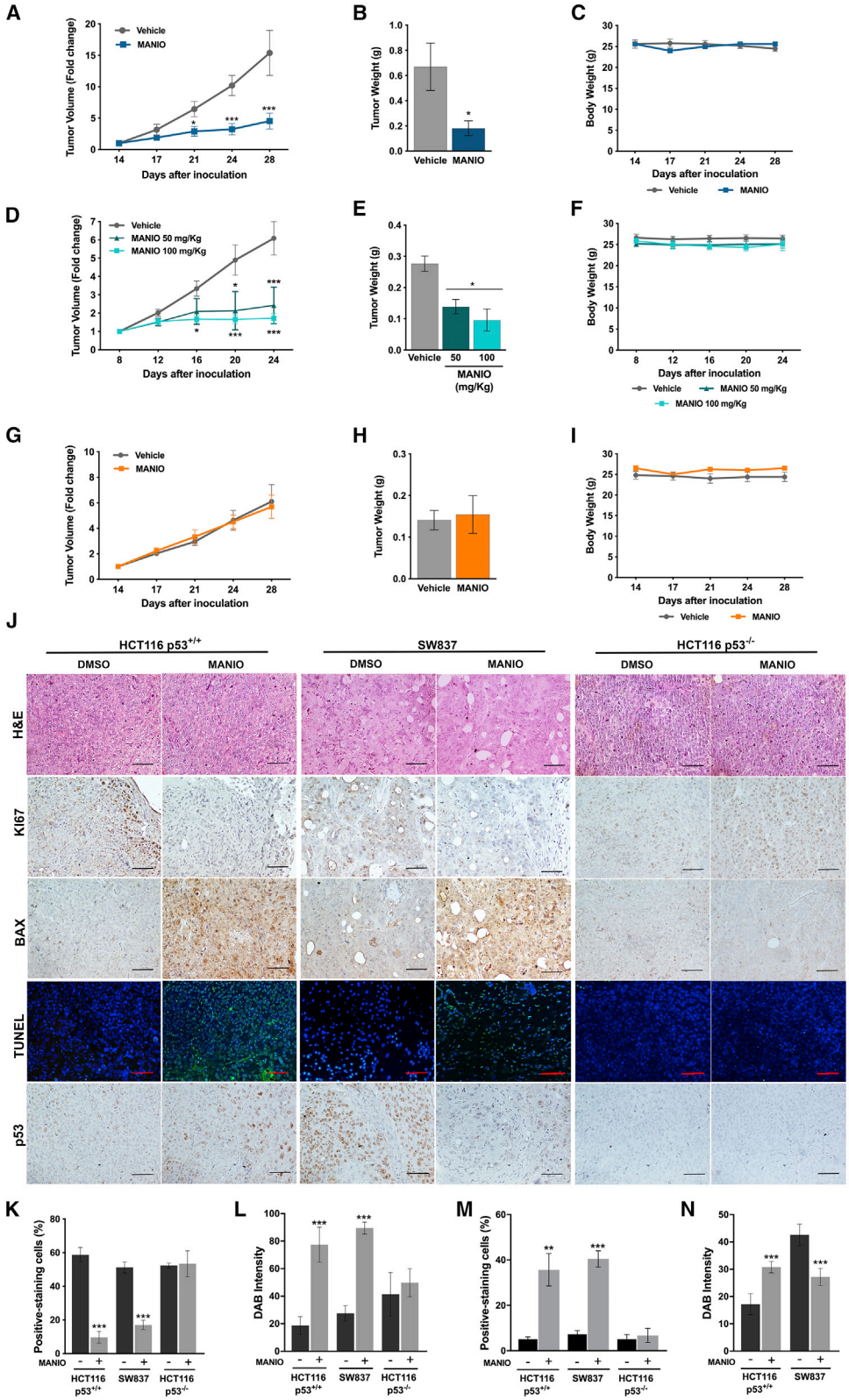

(legend on next page)

mutp53 with high clinical prevalence. This indicated that the binding mode of MANIO may occur irrespective of the formation of particular pockets derived from specific mutation sites, as observed with the binding of Phikan083 to mutp53 Y220C (Boeckler et al., 2008). Interestingly, MANIO was highly effective against mutations with particular interest in a CRC context, namely on R248Q and R248W mutations that have similar frequencies and may exhibit GOF in CRC (Schulz-Heddergott et al., 2018). In fact, cancer patients carrying mutp53 R248Q/W have been associated with lower survival rates than those with other mutp53 forms (Schulz-Heddergott et al., 2018). mutp53 R248Q GOF accelerated tumor onset (Hanel et al., 2013), and knockin mice exhibited a broader tumor spectrum, shorter overall survival, and metastasis formation (Schulz-Heddergott et al., 2018). Mutp53 R248W also interacted with nuclease Mre11, suppressing the binding of the Mre11–Rad50–NBS1 complex to DNA double-stranded breaks, and subsequently inhibiting ataxia-telangiectasia mutated (ATM)-dependent DNA repair (Song et al., 2007). Here, we showed the restoration of the WT-like DNA-binding ability and transactivation function of mutp53 R248W by MANIO, with subsequent upregulation of p53 transcriptional targets involved in cell-cycle arrest (p21) and apoptosis (BAX and PUMA). As with WTp53, the direct interaction of MANIO with mutp53 R248W, leading to its thermal stability, was also demonstrated. Importantly, molecular docking (MD) simulations and cluster analysis to the complex of WTp53 DBD and mutp53 R248W DBD with MANIO (fully described in Method details) showed that this ligand binds to a pocket formed between one dimer of the WTp53 DBD protein and the minor groove of the DNA molecule (Figure S6A). MANIO interacts with the WTp53 DBD protein backbone through hydrogen bonds between its hydroxyl groups and the amide backbone groups of methionine 243 of chain A (M243A) and methionine 243 of chain B (M243B) (each belong to a different monomer). The remaining interactions of MANIO are stacking interactions made with the bases of DNA (DG8, DG12) (Figure S6A). In the case of the mutp53 R248W, in most clusters, the ligand makes a hydrogen bond between one of its hydroxyl oxygen atoms and the W248 side-chain nitrogen. The ligand phenyl group is close to the DNA bases adenine 6 and thymine 7 (Figure S6B). These results prompted us to realize that ligands with a flexible T shape conformation are able to fit perfectly between the DNA molecule and the protein pocket at the dimer interface in a stable way (Sun et al., 2012). Therefore, we anticipate a mechanism of p53 activation by MANIO as a bridging molecule between p53 and DNA, which may eventually compensate for the loss of direct contacts between lysine 248 residue and the DNA. However, it must be noted that the ability of MANIO to promote the proper folding of structural p53 mutants, such as R175H, remains to be addressed.

The p53-dependent antitumor activity of MANIO was further confirmed in CRC xenograft mouse models. In fact, in tumors expressing WT- or mutp53, MANIO inhibited tumor cell proliferation and induced apoptosis, while it did not significantly interfere with the growth of p53 knockout tumors. Interestingly, in accordance with the WTp53 stabilization observed in CRC cells, a marked increase in the p53 levels was also observed in WTp53-expressing tumor tissues treated with MANIO. However, in mutp53-expressing tumor tissues, MANIO significantly reduced the levels of mutp53. Of note, much higher levels of p53 could be observed in control tumors expressing mutp53 compared to those expressing WTp53. Although the mechanism of mutp53 accumulation in tumors remains not fully understood, the disruption of the p53-MDM2 loop can constitute a potential explanation. Actually, the inability of mutp53 to transcriptionally induce MDM2 and of MDM2 to interact and degrade mutp53 in cancer cells greatly reduces the overall mutp53 degradation by ubiquitination (Yue et al., 2017). In fact, mutp53 accumulation in tumors has been considered critical for the occurrence of mutp53 GOF, contributing to the development of more advanced tumors. As such, lower mutp53 levels have been correlated with improved survival rates (Huang et al., 2014), strongly supporting the depletion of mutp53 as a positive marker of cancer therapeutic response (Yue et al., 2017). The restoration of the WT-like function to mutp53 by MANIO, with reestablishment of the p53-MDM2 feedback loop, may explain the reduction in mutp53 expression to similar levels to WTp53-expressing tumor tissues.

No signs of toxicity or morbidity were noticed in MANIO-treated mice. Consistently, MANIO showed much lower growth-inhibitory activity in normal colon cells. In fact, in the case of WTp53 activators, it would be expected that these agents may also activate p53 in normal cells, exhibiting undesirable toxic side effects. Nonetheless, some authors have shown that normal tissues were not significantly affected by genetic re-establishment of p53 (Christophorou et al., 2005). In particular, it was demonstrated that p53-activating signals triggered by acute radiation injury in normal radiosensitive tissues rapidly attenuated, as the damage was promptly resolved.

Figure 5. MANIO has *in vivo* p53-dependent antitumor activity by inhibiting proliferation and enhancing apoptosis

(A–I) Swiss nude mice carrying HCT116 $p53^{+/+}$ (A–C), SW837 (D–F), and HCT116 $p53^{-/-}$ (G–I) xenografts were treated intraperitoneally with 50 or 100 mg/kg MANIO or vehicle (control), twice per week during 2 weeks (6 animals/group); values significantly different from vehicle: $^{*}p < 0.05$, $^{***}p < 0.001$; 2-way ANOVA with Dunnett's multiple comparisons test. Tumor weight of mice carrying HCT116 $p53^{+/+}$ (B), SW837 (E), and HCT116 $p53^{-/-}$ (H) xenografts, at the end of the treatment with MANIO or vehicle; data are means ± SEMs; values significantly different from vehicle: $^{*}p < 0.05$; unpaired Student's t test. Body weight of mice carrying HCT116 $p53^{+/+}$ (C), SW837 (F), and HCT116 $p53^{-/-}$ (I) xenografts during MANIO or vehicle treatment; no significant differences between vehicle and MANIO-treated mice: $p > 0.05$; 2-way ANOVA with Dunnett's multiple comparisons test.

(J) Representative images of Ki67, BAX, DNA fragmentation (TUNEL), and p53 detection in tumor tissues of HCT116 $p53^{+/+}$, SW837, and HCT116 $p53^{-/-}$ xenografts treated with MANIO or vehicle, collected at the end of the treatment (scale bar, 10 μm; magnification × 200).

(K) Percentage of positive-staining Ki67 cells.

(L) Quantification of BAX staining evaluated by 3,3′-diaminobenzidine (DAB) intensity.

(M) Percentage of positive-staining TUNEL cells.

(N) Quantification of p53 staining evaluated by DAB intensity.

In (K)–(N), data are means ± SEMs of 3 independent experiments; values significantly different from vehicle: $^{**}p < 0.01$; $^{***}p < 0.001$; unpaired Student's t test.

The antitumor potential of MANIO through the activation of a p53 pathway was further validated in patient-derived CRC cells. In fact, MANIO upregulated the mRNA levels of several p53 transcriptional targets involved in cell-cycle arrest and apoptosis, while downregulating genes involved in angiogenesis (*VEGF*) and cancer development and chemoresistance (*BIRC5*/Survivin). Survivin plays a crucial role in the pathogenesis of CRC (Williams et al., 2003), being its upregulation associated with poor prognosis (Huang et al., 2013) and resistance of tumor cells to radiotherapy and chemotherapy (Waligórska-Stachura et al., 2012). As such, downregulation of survivin levels by MANIO will improve the CRC therapeutic response.

Importantly, MANIO displayed its highest antiproliferative effect on cells derived from a metastatic CRC patient (CCZ2), previously subjected to standard therapeutic regimens (5-FU, oxaliplatin) combined with the anti-angiogenic agent bevacizumab. MANIO also showed marked antitumor activity against patient-derived cells expressing the missense p53 DBD mutation P151S (CCA8). Although not being a hotspot *TP53* mutation, its clinical relevance should not be disregarded, since its occurrence within the exon 5 of *TP53* is associated with worse outcomes in proximal colon cancers (Russo et al., 2005).

CRC treatments have encompassed the use of conventional chemotherapeutic drugs, including 5-FU, platinum-based agents, and topoisomerases inhibitors (Cremolini et al., 2015). Their combination with targeted therapy has greatly improved the median overall survival of CRC patients, minimizing toxicity and counteracting frequent drug resistance (Yau, 2019). Here, we revealed that low doses of MANIO had synergistic effects with DOXO, 5-FU, and CISP, in immortalized and patient-derived CRC cells. These DNA-damaging drugs are highly dependent on functional p53 to trigger cell death, therefore benefiting CRC patients harboring mutp53 (Russo et al., 2005; Iacopetta, 2003). This study also revealed promising synergistic effects of MANIO in patient-derived CRC cells expressing WTp53. In fact, most of the DNA-damaging agents generally promote post-translational modifications of p53 in its C-terminal and N-terminal, preventing p53 degradation and causing its accumulation (Appella and Anderson, 2001). p53 activators, including MANIO, can act as a thermodynamic stabilizer of the WT DBD conformation, increasing p53 activity and subsequently triggering an apoptotic cell death and modifying factors that are involved in the therapeutic response. In the particular case of MANIO, it may be related, for example, to its ability to increase the levels of Bax, while decreasing survivin in WTp53-expressing patient-derived CRC cells.

This work also shows that MANIO has adequate drug-likeness and pharmacokinetic properties for its clinical translation. Even though MANIO exhibited poor solubility in low pH aqueous solvents, indicating pH-dependent solubility, this limitation can be overcome using pharmaceutically acceptable counter ions that can provide favorable pH conditions upon dissolution in water. This may render the pH of resulting solution closer to the maximum pH of the compound, translating into better absorption rates (Kalepu and Nekkanti, 2015). In fact, many approved orally administered anticancer drugs exhibit this pH-dependent solubility, and the oral bioavailability of these agents was significantly influenced when co-administered with acid-reducing agents (e.g., proton pump inhibitors, H2-receptor antagonists, antacids) (Budha et al., 2012). Salt forms of the compounds may also avoid pH adjustments necessary for their solubilization, as salt formation can improve the crystallinity, stability, and pharmaceutical processing of drugs (Kalepu and Nekkanti, 2015; Béni et al., 2007). MANIO efflux in intestinal epithelium can constitute an additional limitation for oral administration, due to overexpression of the drug efflux pump P-glycoprotein (P-gp). In fact, P-gp is frequently overexpressed in the intestinal epithelium, where it can limit the oral bioavailability of anticancer drugs. Several P-gp inhibitors, such as tariquidar, elacridar, and ONT093, have advanced to clinical development in combination therapy to increase the oral bioavailability of anticancer drugs (Dash et al., 2017).

In conclusion, compelling evidence is herein provided supporting the therapeutic potential of MANIO as an anticancer drug candidate in personalized cancer treatment, particularly of CRC, either as a single agent or in combination with conventional chemotherapeutics.

STAR★METHODS

Detailed methods are provided in the online version of this paper and include the following:

- KEY RESOURCES TABLE
- RESOURCE AVAILABILITY
  - Lead contact
  - Materials availability
  - Data and code availability
- EXPERIMENTAL MODEL AND SUBJECT DETAILS
  - Human cell lines
  - Patient-derived CRC cells
  - Animals
- METHOD DETAILS
  - Compounds
  - Cell viability and proliferation assays
  - Transient transfection of mutp53 in human H1299 tumor cells
  - Cell cycle and apoptosis analysis
  - Western blot analysis
  - Cycloheximide (CHX) assay
  - RNA extraction and RT-qPCR
  - Chromatin immunoprecipitation (ChIP) assay
  - RNA sequencing (RNA-seq)
  - p53 siRNA
  - Cellular thermal shift assay (CETSA)
  - Comet assay
  - Micronucleus test
  - Recombinant human wt and mutp53 R248W DBD protein production
  - Protein-ligand interaction by fluorescence quenching
  - *In vivo* antitumor and toxicity assays
  - Immunohistochemistry (IHC)
  - Combination therapy assays
  - Drug pharmacokinetic (PK) studies
  - *In vitro* PK assays
  - *In vivo* PK assays

- Animal dosing design - *in vivo* PK, non-fasted animals
- MANIO formulation
- Plasma sample collection from mice
- Quantitative bioanalysis (plasma)
- Pharmacokinetics
- Modeling
- Molecular docking
- Molecular dynamics (MD) simulations

● QUANTIFICATION AND STATISTICAL ANALYSIS

SUPPLEMENTAL INFORMATION

Supplemental information can be found online at https://doi.org/10.1016/j.celrep.2021.108982.

ACKNOWLEDGMENTS

We thank PT national funds (FCT/MCTES, Fundação para a Ciência e a Tecnologia, and Ministério da Ciência, Tecnologia e Ensino Superior) through grants UIDB/50006/2020, UID/BIO/04469/2019, UIDB/04539/2020, and UIDP/04539/2020 (CIBB); BioTecNorte operation (NORTE-01-0145-FEDER-000004) and Porto Neurosciences and Neurologic Disease Research Initiative at I3S (Norte-01-0145-FEDER-000008) funded by the European Regional Development Fund under the scope of Norte2020 - Programa Operacional Regional do Norte; Masaryk University (Project MUNI/A/1127/2019) and Ministry of Education, Youth and Sports of the Czech Republic (project nos. LQ1605 and LM2018125); FCT financial support through the fellowships SFRH/BD/119144/2016 (H.R.) and SFRH/BD/117949/2016 (L.R.); Fondazione AIRC (IG#18985, A.I.); and the Programa Operacional Potencial Humano (POCH), specifically the BiotechHealth Programme (Doctoral Programme on Cellular and Molecular Biotechnology Applied to Health Sciences, PD/00016/2012). We thank Dario Rizzotto for assistance in preparing the libraries for RNA sequencing. Funding: This work was supported by PT National Funds (FCT/MCTES, Fundação para a Ciência e Tecnologia, and Ministério da Ciência, Tecnologia e Ensino Superior) via the projects UIDB/50006/2020 (LAQV/REQUIMTE), UIDB/00313/2020, and UIDP/00313/2020, co-funded by COMPETE2020-UE.

AUTHOR CONTRIBUTIONS

Conception and design, H.R. and L.S.; development of methodology, H.R., J.S., L.R., J.C., M.I.L.S., C.G., F.R., P.C., R.V., B.B., and S.P.; resources (patient-derived tumor tissues), P.V. and P.F.; analysis and interpretation of data, H.R., A.I., T.M.V.D.P.M., and L.S.; writing – original draft, H.R. and L.S.; writing – review and editing, all authors; project administration, T.M.V.D.P.M. and L.S.

DECLARATION OF INTERESTS

One patent application protecting the compound MANIO disclosed in this manuscript has been filed by the following authors: H.R., M.I.L.S., T.M.V.D.P.M., and L.S.

Received: July 30, 2020
Revised: March 8, 2021
Accepted: March 22, 2021
Published: April 13, 2021

REFERENCES

Alessandrini, F., Pezzè, L., Menendez, D., Resnick, M.A., and Ciribilli, Y. (2018). ETV7-Mediated DNAJC15 Repression Leads to Doxorubicin Resistance in Breast Cancer Cells. Neoplasia *20*, 857–870.

Appella, E., and Anderson, C.W. (2001). Post-translational modifications and activation of p53 by genotoxic stresses. Eur. J. Biochem. *268*, 2764–2772.

Araghi, M., Soerjomataram, I., Bardot, A., Ferlay, J., Cabasag, C.J., Morrison, D.S., De, P., Tervonen, H., Walsh, P.M., Bucher, O., et al. (2019). Changes in colorectal cancer incidence in seven high-income countries: a population-based study. Lancet Gastroenterol. Hepatol. *4*, 511–518.

Banker, M.J., Clark, T.H., and Williams, J.A. (2003). Development and validation of a 96-well equilibrium dialysis apparatus for measuring plasma protein binding. J. Pharm. Sci. *92*, 967–974.

Béni, S., Szakács, Z., Csernák, O., Barcza, L., and Noszál, B. (2007). Cyclodextrin/imatinib complexation: binding mode and charge dependent stabilities. Eur. J. Pharm. Sci. *30*, 167–174.

Boeckler, F.M., Joerger, A.C., Jaggi, G., Rutherford, T.J., Veprintsev, D.B., and Fersht, A.R. (2008). Targeted rescue of a destabilized mutant of p53 by an in silico screened drug. Proc. Natl. Acad. Sci. USA *105*, 10360–10365.

Budha, N.R., Frymoyer, A., Smelick, G.S., Jin, J.Y., Yago, M.R., Dresser, M.J., Holden, S.N., Benet, L.Z., and Ware, J.A. (2012). Drug absorption interactions between oral targeted anticancer agents and PPIs: is pH-dependent solubility the Achilles heel of targeted therapy? Clin. Pharmacol. Ther. *92*, 203–213.

Chou, T.C., and Talalay, P. (1984). Quantitative analysis of dose-effect relationships: the combined effects of multiple drugs or enzyme inhibitors. Adv. Enzyme Regul. *22*, 27–55.

Christophorou, M.A., Martin-Zanca, D., Soucek, L., Lawlor, E.R., Brown-Swigart, L., Verschuren, E.W., and Evan, G.I. (2005). Temporal dissection of p53 function in vitro and in vivo. Nat. Genet. *37*, 718–726.

Cremolini, C., Schirripa, M., Antoniotti, C., Moretto, R., Salvatore, L., Masi, G., Falcone, A., and Loupakis, F. (2015). First-line chemotherapy for mCRC—a review and evidence-based algorithm. Nat. Rev. Clin. Oncol. *12*, 607–619.

Darden, T., York, D., and Pedersen, L. (1993). Particle mesh Ewald: an N·log(N) method for Ewald sums in large systems. J. Chem. Phys. *98*, 10089–10092.

Dash, R.P., Jayachandra Babu, R., and Srinivas, N.R. (2017). Therapeutic Potential and Utility of Elacridar with Respect to P-glycoprotein Inhibition: An Insight from the Published In Vitro, Preclinical and Clinical Studies. Eur. J. Drug Metab. Pharmacokinet. *42*, 915–933.

Dekker, E., Tanis, P.J., Vleugels, J.L.A., Kasi, P.M., and Wallace, M.B. (2019). Colorectal cancer. Lancet *394*, 1467–1480.

Dobin, A., Davis, C.A., Schlesinger, F., Drenkow, J., Zaleski, C., Jha, S., Batut, P., Chaisson, M., and Gingeras, T.R. (2013). STAR: ultrafast universal RNA-seq aligner. Bioinformatics *29*, 15–21.

Engeland, K. (2018). Cell cycle arrest through indirect transcriptional repression by p53: I have a DREAM. Cell Death Differ. *25*, 114–132.

Fernandes, C., Palmeira, A., Ramos, I.I., Carniero, C., Afonso, C., Tiritan, M.E., Cidade, H., Pinto, P.C.A.G., Saraiva, M.L.M.F.S., Reis, S., and Pinto, M.M.M. (2017). Chiral Derivatives of Xanthones: Investigation of the Effect of Enantioselectivity on Inhibition of Cyclooxygenases (COX-1 and COX-2) and Binding Interaction with Human Serum Albumin. Pharmaceuticals (Basel) *10*, 50.

Fischer, M. (2017). Census and evaluation of p53 target genes. Oncogene *36*, 3943–3956.

Gomes, A.S., Trovão, F., Andrade Pinheiro, B., Freire, F., Gomes, S., Oliveira, C., Domingues, L., Romão, M.J., Saraiva, L., and Carvalho, A.L. (2018). The Crystal Structure of the R280K Mutant of Human p53 Explains the Loss of DNA Binding. Int. J. Mol. Sci. *19*, 1184.

Gomes, S., Bosco, B., Loureiro, J.B., Ramos, H., Raimundo, L., Soares, J., Nazareth, N., Barcherini, V., Domingues, L., Oliveira, C., et al. (2019). SLMP53-2 Restores Wild-Type-Like Function to Mutant p53 through Hsp70: Promising Activity in Hepatocellular Carcinoma. Cancers (Basel) *11*, 1151.

Gomes, A.S., Ramos, H., Gomes, S., Loureiro, J.B., Soares, J., Barcherini, V., Monti, P., Fronza, G., Oliveira, C., Domingues, L., et al. (2020). SLMP53-1 interacts with wild-type and mutant p53 DNA-binding domain and reactivates multiple hotspot mutations. Biochim. Biophys. Acta, Gen. Subj. *1864*, 129440.

Gyori, B.M., Venkatachalam, G., Thiagarajan, P.S., Hsu, D., and Clement, M.V. (2014). OpenComet: an automated tool for comet assay image analysis. Redox Biol. *2*, 457–465.

Hanel, W., Marchenko, N., Xu, S., Yu, S.X., Weng, W., and Moll, U. (2013). Two hot spot mutant p53 mouse models display differential gain of function in tumorigenesis. Cell Death Differ. *20*, 898–909.

Hidalgo, I.J., Raub, T.J., and Borchardt, R.T. (1989). Characterization of the human colon carcinoma cell line (Caco-2) as a model system for intestinal epithelial permeability. Gastroenterology *96*, 736–749.

Hornak, V., Abel, R., Okur, A., Strockbine, B., Roitberg, A., and Simmerling, C. (2006). Comparison of multiple Amber force fields and development of improved protein backbone parameters. Proteins *65*, 712–725.

Huang, Y.J., Qi, W.X., He, A.N., Sun, Y.J., Shen, Z., and Yao, Y. (2013). The prognostic value of survivin expression in patients with colorectal carcinoma: a meta-analysis. Jpn. J. Clin. Oncol. *43*, 988–995.

Huang, K., Chen, L., Zhang, J., Wu, Z., Lan, L., Wang, L., Lu, B., and Liu, Y. (2014). Elevated p53 expression levels correlate with tumor progression and poor prognosis in patients exhibiting esophageal squamous cell carcinoma. Oncol. Lett. *8*, 1441–1446.

Iacopetta, B. (2003). TP53 mutation in colorectal cancer. Hum. Mutat. *21*, 271–276.

International Agency for Research on Cancer; World Health Organization (2019). Global Cancer Observatory. https://gco.iarc.fr/.

Jabs, J., Zickgraf, F.M., Park, J., Wagner, S., Jiang, X., Jechow, K., Kleinheinz, K., Toprak, U.H., Schneider, M.A., Meister, M., et al. (2017). Screening drug effects in patient-derived cancer cells links organoid responses to genome alterations. Mol. Syst. Biol. *13*, 955.

Kalepu, S., and Nekkanti, V. (2015). Insoluble drug delivery strategies: review of recent advances and business prospects. Acta Pharm. Sin. B *5*, 442–453.

Khaleel, S.A., Al-Abd, A.M., Ali, A.A., and Abdel-Naim, A.B. (2016). Didox and resveratrol sensitize colorectal cancer cells to doxorubicin via activating apoptosis and ameliorating P-glycoprotein activity. Sci. Rep. *6*, 36855.

Kitayner, M., Rozenberg, H., Kessler, N., Rabinovich, D., Shaulov, L., Haran, T.E., and Shakked, Z. (2006). Structural basis of DNA recognition by p53 tetramers. Mol. Cell *22*, 741–753.

Kocik, J., Machula, M., Wisniewska, A., Surmiak, E., Holak, T.A., and Skalniak, L. (2019). Helping the Released Guardian: Drug Combinations for Supporting the Anticancer Activity of HDM2 (MDM2) Antagonists. Cancers (Basel) *11*, 1014.

Kuleshov, M.V., Jones, M.R., Rouillard, A.D., Fernandez, N.F., Duan, Q., Wang, Z., Koplev, S., Jenkins, S.L., Jagodnik, K.M., Lachmann, A., et al. (2016). Enrichr: a comprehensive gene set enrichment analysis web server 2016 update. Nucleic Acids Res. *44* (*W1*), W90–W97.

Li, X.L., Zhou, J., Chen, Z.R., and Chng, W.J. (2015). P53 mutations in colorectal cancer - molecular pathogenesis and pharmacological reactivation. World J. Gastroenterol. *21*, 84–93.

Li, X., Xu, Y., Cui, H., Huang, T., Wang, D., Lian, B., Li, W., Qin, G., Chen, L., and Xie, L. (2017). Prediction of synergistic anti-cancer drug combinations based on drug target network and drug induced gene expression profiles. Artif. Intell. Med. *83*, 35–43.

Li, Y., Wang, Z., Chen, Y., Petersen, R.B., Zheng, L., and Huang, K. (2019). Salvation of the fallen angel: reactivating mutant p53. Br. J. Pharmacol. *176*, 817–831.

Lipinski, C.A., Lombardo, F., Dominy, B.W., and Feeney, P.J. (2001). Experimental and computational approaches to estimate solubility and permeability in drug discovery and development settings. Adv. Drug Deliv. Rev. *46*, 3–26.

Love, M.I., Huber, W., and Anders, S. (2014). Moderated estimation of fold change and dispersion for RNA-seq data with DESeq2. Genome Biol. *15*, 550.

Lu, T., Zou, Y., Xu, G., Potter, J.A., Taylor, G.L., Duan, Q., Yang, Q., Xiong, H., Qiu, H., Ye, D., et al. (2016). PRIMA-1Met suppresses colorectal cancer independent of p53 by targeting MEK. Oncotarget *7*, 83017–83030.

Martinez Molina, D., and Nordlund, P. (2016). The Cellular Thermal Shift Assay: A Novel Biophysical Assay for In Situ Drug Target Engagement and Mechanistic Biomarker Studies. Annu. Rev. Pharmacol. Toxicol. *56*, 141–161.

Merkel, O., Taylor, N., Prutsch, N., Staber, P.B., Moriggl, R., Turner, S.D., and Kenner, L. (2017). When the guardian sleeps: reactivation of the p53 pathway in cancer. Mutat. Res. *773*, 1–13.

Miyamoto, S., and Kollman, P.A. (1992). Settle: an analytical version of the SHAKE and RATTLE algorithm for rigid water models. J. Comput. Chem. *13*, 952–962.

Morris, G.M., Goodsell, D.S., Halliday, R.S., Huey, R., Hart, W.E., Belew, R.K., and Olson, A.J. (1998). Automated docking using a Lamarckian genetic algorithm and an empirical binding free energy function. J. Comput. Chem. *19*, 1639–1662.

Muller, P.A., and Vousden, K.H. (2014). Mutant p53 in cancer: new functions and therapeutic opportunities. Cancer Cell *25*, 304–317.

Nakayama, M., and Oshima, M. (2019). Mutant p53 in colon cancer. J. Mol. Cell Biol. *11*, 267–276.

Obach, R.S., Baxter, J.G., Liston, T.E., Silber, B.M., Jones, B.C., MacIntyre, F., Rance, D.J., and Wastall, P. (1997). The prediction of human pharmacokinetic parameters from preclinical and in vitro metabolism data. J. Pharmacol. Exp. Ther. *283*, 46–58.

Raimundo, L., Espadinha, M., Soares, J., Loureiro, J.B., Alves, M.G., Santos, M.M.M., and Saraiva, L. (2018). Improving anticancer activity towards colon cancer cells with a new p53-activating agent. Br. J. Pharmacol. *175*, 3947–3962.

Russo, A., Bazan, V., Iacopetta, B., Kerr, D., Soussi, T., and Gebbia, N.; TP53-CRC Collaborative Study Group (2005). The TP53 colorectal cancer international collaborative study on the prognostic and predictive significance of p53 mutation: influence of tumor site, type of mutation, and adjuvant treatment. J. Clin. Oncol. *23*, 7518–7528.

Salim, K.Y., Maleki Vareki, S., Danter, W.R., and Koropatnick, J. (2016). COTI-2, a novel small molecule that is active against multiple human cancer cell lines in vitro and in vivo. Oncotarget *7*, 41363–41379.

Sangster, J. (1997). Octanol-Water Partition Coefficients: Fundamentals and Physical Chemistry (John Wiley & Sons).

Schindelin, J., Rueden, C.T., Hiner, M.C., and Eliceiri, K.W. (2015). The ImageJ ecosystem: an open platform for biomedical image analysis. Mol. Reprod. Dev. *82*, 518–529.

Schneider, C.A., Rasband, W.S., and Eliceiri, K.W. (2012). NIH Image to ImageJ: 25 years of image analysis. Nat. Methods *9*, 671–675.

Schulz-Heddergott, R., Stark, N., Edmunds, S.J., Li, J., Conradi, L.C., Bohnenberger, H., Ceteci, F., Greten, F.R., Dobbelstein, M., and Moll, U.M. (2018). Therapeutic Ablation of Gain-of-Function Mutant p53 in Colorectal Cancer Inhibits Stat3-Mediated Tumor Growth and Invasion. Cancer Cell *34*, 298–314.e7.

Soares, M.I., Brito, A.F., Laranjo, M., Paixão, J.A., Botelho, M.F., and Pinho e Melo, T.M. (2013). Chiral 6,7-bis(hydroxymethyl)-1H,3H-pyrrolo[1,2-c]thiazoles with anti-breast cancer properties. Eur. J. Med. Chem. *60*, 254–262.

Soares, J., Raimundo, L., Pereira, N.A., dos Santos, D.J., Pérez, M., Queiroz, G., Leão, M., Santos, M.M., and Saraiva, L. (2015). A tryptophanol-derived oxazolopiperidone lactam is cytotoxic against tumors via inhibition of p53 interaction with murine double minute proteins. Pharmacol. Res. *95-96*, 42–52.

Soares, J., Raimundo, L., Pereira, N.A., Monteiro, Â., Gomes, S., Bessa, C., Pereira, C., Queiroz, G., Bisio, A., Fernandes, J., et al. (2016). Reactivation of wild-type and mutant p53 by tryptophanol derived oxazoloisoindolinone SLMP53-1, a novel anticancer small-molecule. Oncotarget *7*, 4326–4343.

Soares, J., Espadinha, M., Raimundo, L., Ramos, H., Gomes, A.S., Gomes, S., Loureiro, J.B., Inga, A., Reis, F., Gomes, C., et al. (2017). DIMP53-1: a novel small-molecule dual inhibitor of p53-MDM2/X interactions with multifunctional p53-dependent anticancer properties. Mol. Oncol. *11*, 612–627.

Song, H., Hollstein, M., and Xu, Y. (2007). p53 gain-of-function cancer mutants induce genetic instability by inactivating ATM. Nat. Cell Biol. *9*, 573–580.

Sramek, M., Neradil, J., Macigova, P., Mudry, P., Polaskova, K., Slaby, O., Noskova, H., Sterba, J., and Veselska, R. (2018). Effects of Sunitinib and Other Kinase Inhibitors on Cells Harboring a *PDGFRB* Mutation Associated with Infantile Myofibromatosis. Int. J. Mol. Sci. *19*, 2599.

Sun, H., Tawa, G., and Wallqvist, A. (2012). Classification of scaffold-hopping approaches. Drug Discov. Today *17*, 310–324.

Tan, B.X., Brown, C.J., Ferrer, F.J., Yuen, T.Y., Quah, S.T., Chan, B.H., Jansson, A.E., Teo, H.L., Nordlund, P., and Lane, D.P. (2015). Assessing the Efficacy of Mdm2/Mdm4-Inhibiting Stapled Peptides Using Cellular Thermal Shift Assays. Sci. Rep. *5*, 12116.

The Cancer Genome Atlas Network (2012). Comprehensive molecular characterization of human colon and rectal cancer. Nature *487*, 330–337.

Toutain, P.L., and Bousquet-Mélou, A. (2004). Volumes of distribution. J. Vet. Pharmacol. Ther. *27*, 441–453.

Undevia, S.D., Gomez-Abuin, G., and Ratain, M.J. (2005). Pharmacokinetic variability of anticancer agents. Nat. Rev. Cancer *5*, 447–458.

Vousden, K.H., and Prives, C. (2009). Blinded by the Light: The Growing Complexity of p53. Cell *137*, 413–431.

Waligórska-Stachura, J., Jankowska, A., Waśko, R., Liebert, W., Biczysko, M., Czarnywojtek, A., Baszko-Błaszyk, D., Shimek, V., and Ruchała, M. (2012). Survivin–prognostic tumor biomarker in human neoplasms–review. Ginekol. Pol. *83*, 537–540.

Wang, J., Wolf, R.M., Caldwell, J.W., Kollman, P.A., and Case, D.A. (2004). Development and testing of a general amber force field. J. Comput. Chem. *25*, 1157–1174.

Williams, N.S., Gaynor, R.B., Scoggin, S., Verma, U., Gokaslan, T., Simmang, C., Fleming, J., Tavana, D., Frenkel, E., and Becerra, C. (2003). Identification and validation of genes involved in the pathogenesis of colorectal cancer using cDNA microarrays and RNA interference. Clin. Cancer Res. *9*, 931–946.

Yau, T.O. (2019). Precision treatment in colorectal cancer: now and the future. JGH Open *3*, 361–369.

Yue, X., Zhao, Y., Xu, Y., Zheng, M., Feng, Z., and Hu, W. (2017). Mutant p53 in Cancer: Accumulation, Gain-of-Function, and Therapy. J. Mol. Biol. *429*, 1595–1606.

STAR★METHODS

KEY RESOURCES TABLE

REAGENT or RESOURCE	SOURCE	IDENTIFIER
Antibodies		
BAX (6A7) (Mouse monoclonal)	Thermo Scientific	Cat# MA5-14003; RRID: AB_626728
BCL-2 (C-2) (Mouse monoclonal)	Santa Cruz Biotechnology	Cat# sc-7382; RRID: AB_626736
CLEAVED PARP (C2-10) (Mouse monoclonal)	Santa Cruz Biotechnology	Cat# sc-53643; RRID: AB_785086
GADD45 alpha (Rabbit polyclonal)	Merck Millipore	Cat# ABE2696
GAPDH (6C5) (Mouse monoclonal)	Santa Cruz Biotechnology	Cat# sc-32233; RRID: AB_627679
KI67 (SP6) (Rabbit monoclonal)	Thermo Scientific	Cat# MA5-14520; RRID: AB_10979488
KILLER/DR5 (D-6) (Mouse monoclonal)	Santa Cruz Biotechnology	Cat# sc-166624; RRID: AB_2204942
MDM2 (SMP14) (Mouse monoclonal)	Santa Cruz Biotechnology	Cat# sc-965; RRID: AB_627920
Normal mouse IgG immunoglobulin	Santa Cruz Biotechnology	Cat# sc-2025; RRID: AB_737182
p21 (C-19) (Rabbit polyclonal)	Santa Cruz Biotechnology	Cat# sc-397; RRID: AB_632126
p53 (DO-1) (Mouse monoclonal)	Santa Cruz Biotechnology	Cat# sc-126; RRID: AB_628082
PUMA (B-6) (Mouse monoclonal)	Santa Cruz Biotechnology	Cat# sc-377015; RRID: AB_2714161
Anti-mouse HRP-conjugated	Santa Cruz Biotechnology	Cat# sc-2005; RRID: AB_631736
Anti-rabbit HRP-conjugated	Santa Cruz Biotechnology	Cat# sc-2004; RRID: AB_631746
Bacterial strains		
Escherichia coli BL21 (DE3)	NZYTech	Cat# MB00401
Biological samples		
Patient-derived colorectal cancer cells	This paper	N/A
Chemicals, peptides, and recombinant proteins		
Doxorubicin	Sigma-Aldrich	Cat# D1515
Etoposide	Calbiochem	Cat# 80055-248
Cisplatin	Enzo Life Science	Cat# BML-GR356
5-Fluorouracil	Enzo Life Science	Cat# ALX-480-099-G005
Penicillin-Streptomycin	Biosera	Cat# XC-A4122
Ciprofloxacin	Merck	Cat# 17850
Piperacillin plus tazobactam	Merck	Cat# P8396
Amphotericin B	Merck	Cat# 171375
Cycloheximide	Sigma-Aldrich	Cat# C4859
Critical commercial assays		
Illustra™ RNAspin Mini RNA Isolation kit	GE Healthcare	Cat# GE25-0500-71
OxiSelect Comet Assay kit	Cell Biolabs	Cat# STA-351
MycoAlert PLUS mycoplasma detection kit	Lonza	Cat# LT07-118
Annexin V-FITC Apoptosis DetectionKKit I	BD Biosciences	Cat#556547
ECL Amersham kit	GE Healthcare	Cat# GERPN2209
Deposited data		
RNA-sequencing data	This paper https://www.ncbi.nlm.nih.gov/geo/query/acc.cgi?acc=GSE145482	GEO: GSE145482
Experimental models: cell lines		
A431	ATCC	ATCC® CRL-1555
H1299	ATCC	ATCC® CRL-5803
NCI-H460	ATCC	ATCC® HTB-177
HCC1937	ATCC	ATCC® CRL-2336
MCF-7	ATCC	ATCC® HTB-22

(*Continued on next page*)

Continued

REAGENT or RESOURCE	SOURCE	IDENTIFIER
MDA-MB-231	ATCC	ATCC® HTB-26
MDA-MB-468	ATCC	ATCC® HTB-132
CCD-18Co	ATCC	ATCC® CRL-1459
HCT116 $p53^{+/+}$	B. Vogelstein, The Johns Hopkins Kimmel Cancer Center, Baltimore, MD, USA	N/A
HCT116 $p53^{-/-}$	B. Vogelstein, The Johns Hopkins Kimmel Cancer Center, Baltimore, MD, USA	N/A
HT-29	ATCC	ATCC® HTB-38
LS-1034	ATCC	ATCC® CL-187
SW837	ATCC	ATCC® CCL-235
IGROV-1	Leonor David, Instituto de Investigação e Inovação em Saúde, Porto, Portugal	N/A
SK-OV-3	Leonor David, Instituto de Investigação e Inovação em Saúde, Porto, Portugal	N/A
Experimental models: organisms/strains		
Female Swiss nude mice	Charles River	N/A
Oligonucleotides		
Primers for qPCR		
B2M FW: AGGCTATCCAGCGTACTCCA	This paper	N/A
B2M RV: ATGGATGAAACCCAGACACA	This paper	N/A
BAX FW: GCTGTTGGGCTGGATCCAAG	This paper	N/A
BAX RV: TCAGCCCATCTTCTTCCAGA	This paper	N/A
BIRC5 FW: GACGACCCCATAGAGGAACAT	This paper	N/A
BIRC5 RV: CGCACTTTCTCCGCAGTTTC	This paper	N/A
BRCA1 FW: CACTCAGCAGAGGGATACCA	This paper	N/A
BRCA1 RV: GAGTTGTTCCTTTGGCCATGT	This paper	N/A
CDKN1A FW: CTGGAGACTCTCAGGGTCGAAA	This paper	N/A
CDKN1A RV: GATTAGGGCTTCCTCTTGGAGAA	This paper	N/A
E2F1 FW: CTACGTGACGTGTCAGGACC	This paper	N/A
E2F1 RV: CTGAAAGTTCTCCGAAGAGTCCA	This paper	N/A
EXO1 FW: GCCTGGCCCAGAAGAAACTT	This paper	N/A
EXO1 RV: CTGGGATTCACTAGTTCTCTCAGAT	This paper	N/A
FANCA FW: TGGAGCTCAAGGGTCAGGG	This paper	N/A
FANCA RV: CCAGCAGCTCTGCCACG	This paper	N/A
GADD45A FW: TCAGCGCACGATCACTGTC	This paper	N/A
GADD45A RV: CCAGCAGGCACAACACCAC	This paper	N/A
GAPDH FW: GGCCAAGGTCATCCATGA	This paper	N/A
GAPDH RV: TCAGTGTAGCCCAGGATG	This paper	N/A
HSP90AB1 FW: CGCATGAAGGAGACACAGAA	This paper	N/A
HSP90AB1 RV: TCCCATCAAATTCCTTGAGC	This paper	N/A
MDM2 FW: GGCCTGCTTTACATGTGCAA	This paper	N/A
MDM2 RV: GCACAATCATTTGAATTGGTTGTC	This paper	N/A
NOXA FW: AGCTGGAAGTCGAGTGTGCT	This paper	N/A
NOXA RV: TCCTGAGCAGAAGAGTTTGGA	This paper	N/A
PUMA FW: CCTGGAGGGTCCTGTACAATCT	This paper	N/A
PUMA RV: GCACCTAATTGGGCTCCATCT	This paper	N/A
TNFRSF10B FW: TGACTCATCTCAGAAATG TCAATTCTTA	This paper	N/A
TNFRSF10B RV: GGACACAAGAAGAAAAC CTTAATGC	This paper	N/A

(*Continued on next page*)

Continued

REAGENT or RESOURCE	SOURCE	IDENTIFIER
VEGF FW: GCTCGGTGCTGGAATTTGAT	This paper	N/A
VEGF RV: TCACTCACTTTGCCCCTGTC	This paper	N/A
YWHAZ1 FW: CAACACATCCTATCAGACTGGG	This paper	N/A
YWHAZ1 RV: AATGTATCAAGTTCAGCAATGGC	This paper	N/A
Primers for ChIP		
ACTIN B FW: TCTCCCTCCTCCTCTTCCTCAAT	This paper	N/A
ACTIN B RV: TCGCGCCGCTGGGTTTTATA	This paper	N/A
CDKN1A FW: GTGGCTCTGATTGGCTTTCTG	This paper	N/A
CDKN1A RV: CTCCTACCATCCCCTTCCTC	This paper	N/A
MDM2 FW: GAGGTCCGGATGATCGCAG	This paper	N/A
MDM2 RV: GGAAAATGCATGGTTTAAATAGCC	This paper	N/A
Recombinant DNA		
pETM20-mutp53	(Gomes et al., 2018)	N/A
Software and algorithms		
GraphPad v7.0	Prism	N/A
STAR v2.5.3a	(Dobin et al., 2013)	N/A
FlowJo v10.0.7	Tree Star	N/A
Image Lab v5.2.1	Bio-Rad Laboratories	N/A
ImageJ v1.50i	(Schneider et al., 2012)	N/A
AutoDock 4.2.6	The Scripps Research Institute	N/A
Lamarckian genetic algorithm	(Morris et al., 1998)	N/A

RESOURCE AVAILABILITY

Lead contact

Further information and requests for resources and reagents should be directed to and will be fulfilled by the lead contact, Lucília Saraiva (lucilia.saraiva@ff.up.pt).

Materials availability

This study did not generate new unique reagents.

Data and code availability

To review GEO accession GSE145482, please go to https://www.ncbi.nlm.nih.gov/geo/query/acc.cgi?acc=GSE145482, and enter token adobywykjvmbpgd into the box.

EXPERIMENTAL MODEL AND SUBJECT DETAILS

Human cell lines

Human cell lines used are described in Key Resources Table; cells were routinely cultured in RPMI-1640 medium with UltraGlutamine (Lonza, VWR), excepting CCD-18Co cells that were cultured in EMEM (Lonza, Ingrenor, Porto, Portugal), supplemented with 10% fetal bovine serum (FBS; GIBCO, Alfagene, Lisboa, Portugal), and maintained at 37°C with 5% CO_2. Cells were routinely tested for mycoplasma infection and recently characterized and authenticated using short tandem repeat DNA profiling.

Patient-derived CRC cells

Patient-derived CRC cell lines are described in Key resources table. Patient gender and age are referred in Table S1. Cells were established from tumor tissue samples with written informed consent approved by the Ethics Committee of the St. Anne's University Hospital Brno (ref. no. 74V/2018) or from tumor tissue samples provided through Bank of Biological Material (Masaryk Memorial Cancer Institute, Brno) which is a part of Biomolecular Resources Research Infrastructure (BBMRI). Tumor tissues pieces were cultured in DMEM complete culture medium supplemented with 10% fetal calf serum, 2 mM glutamine (all from Biosera, Nuaille, France), 100 IU/mL penicillin, 100 μg/mL streptomycin, 10 μg/mL ciprofloxacine, 400 μg/mL piperacilin plus tazobactam, and 1,25 μg/mL amphotericin B (all antibiotics described in Key resources table). Outgrowing cells were then subcultured into complete growth medium with penicillin and streptomycin only.

Animals

Animal experiments were conducted according to the EU Directive 2010/63/EU and to the National Authorities. The study was approved by the local Animal Welfare Body (Ref. ORBEA-5-2016). Female Swiss nude mice (Charles-River Laboratories, Barcelona, Spain) were housed under pathogen-free conditions in ventilated cages. For the *in vivo* antitumor assays, 10 to 12 weeks old mice were used.

METHOD DETAILS

Compounds

MANIO was synthesized as described (Soares et al., 2013). Compounds were dissolved in dimethyl sulfoxide (DMSO; Sigma-Aldrich, Sintra, Portugal), excepting cisplatin that was dissolved in saline. In all experiments, the solvent (0.1 – 0.25% DMSO) was included as control.

Cell viability and proliferation assays

For sulforhodamine B (SRB) assays, cells were seeded in 96-well plates at 4.0×10^3 (NCI-H460), 5.0×10^3 (HCT116, MCF-7, MDA-MB-468, LS-1034, CCD-18Co, HT-29, IGROV-1, A431, and SK-OV-3), 7.5×10^3 (SW837 and H1299) or 1.0×10^4 (HCC1937) cells/well, as reported (Soares et al., 2015). For MTT assays, patient-derived CRC cells were seeded in 96-well plates at 3×10^3 cells/well, as reported (Sramek et al., 2018). Half maximal inhibitory concentration (IC_{50}) values were determined as described (Soares et al., 2015).

For colony formation assays, HCT116 ($p53^{+/+}$ and $p53^{-/-}$) and SW837 cells were seeded in 6-well plates at 1.0×10^3 and 2.5×10^3 cells/well, respectively, and incubated with MANIO for 11-14 days. Formed colonies were fixed, stained and analyzed as reported (Raimundo et al., 2018).

Transient transfection of mutp53 in human H1299 tumor cells

For ectopic expression of mutp53, p53 null H1299 cells were transfected with 75 ng of pcDNA3 mammalian expression vectors encoding full-length human mutp53 (R280K, R175H, G245D, G245S, R248Q, R248W, R273H, R273C, Y220C or R282W), or empty pcDNA3, as described (Gomes et al., 2020).

Cell cycle and apoptosis analysis

HCT116 ($p53^{+/+}$ and $p53^{-/-}$) and SW837 cells were seeded in 6-well plates at 1.5×10^5 or 2.25×10^5 cells/well respectively, for 24 h, followed by treatment with MANIO. Cell cycle and apoptosis were analyzed as reported (Soares et al., 2015; Gomes et al., 2019).

Western blot analysis

HCT116 ($p53^{+/+}$ and $p53^{-/-}$) and SW837 cells were seeded in 6-well plates at 1.5×10^5 and 2.25×10^5 cells/well respectively, and patient-derived CRC cells in ⌀100 mm Petri dishes at 3×10^5 cells/dish, for 24 h, followed by treatment with MANIO. Protein extracts were analyzed as described (Raimundo et al., 2018). Antibodies are listed in Key resources table.

Cycloheximide (CHX) assay

HCT116$p53^{+/+}$ cells were seeded in 6-well plates at 1.5×10^5/well for 24 h, followed by treatment with MANIO. Cells were then treated with 150 μg/mL CHX for up to 4 h. p53 expression was analyzed by western blot as described above.

RNA extraction and RT-qPCR

HCT116 ($p53^{+/+}$ and $p53^{-/-}$) and SW837 cells were seeded in 6-well plates at 1.5×10^5 and 2.25×10^5 cells/well respectively, and patient-derived CRC cells in ⌀100 mm Petri dishes at 3×10^5 cells/dish, for 24 h, followed by treatment with MANIO. For HCT116 and SW837 cells, total RNA extraction and RT-qPCR were performed as described (Soares et al., 2017). For patient-derived CRC cells, total RNA extraction and RT-qPCR were performed as described (Sramek et al., 2018). Primers are listed in Key resources table.

Chromatin immunoprecipitation (ChIP) assay

HCT116 $p53^{+/+}$ and SW837 cells were seeded in 75 cm^2 flasks at 1.5×10^6 and 2.25×10^6 cells/well respectively, for 24 h, and treated with MANIO for additional 24 h. ChIP was performed as described (Alessandrini et al., 2018). Mouse monoclonal anti-p53 antibody was used for immunoprecipitation, and normal mouse IgG immunoglobulin was used as negative control. p53 occupancy at the gene promoters was measured by RT-qPCR. Primers are listed in Key resources table.

RNA sequencing (RNA-seq)

HCT116$p53^{+/+}$ cells were seeded in 75 cm^2 flasks at 1.5×10^6 cells/well, for 24 h, and treated with MANIO. Total RNA was extracted using the Illustra™ RNAspin Mini RNA Isolation Kit (GE Healthcare, Milan, Italy). RNA integrity was checked by the Agilent 2100 Bioanalyzer (Agilent Technologies, Milan, Italy), discarding preparations with RIN (RNA integrity number) values 8. Sequencing libraries were produced following the TruSeq RNA Library kit v2 protocol (Illumina, ThermoFisher) and using 1 μg of RNA as input. All samples were sequenced using HiSeq 2500, obtaining ≈25M raw reads per sample. Raw sequence files were subjected to quality control

analysis using FastQC v1.3 (http://www.bioinformatics.babraham.ac.uk/projects/fastqc/). Transcript quantification was conducted with STAR v2.5.3a (Dobin et al., 2013) (assigned to a gene using the GENCODE annotation v27, using the STAR function "quantMode GeneCounts") mapped to the human genome version GRCh38 and with reference annotation. Read counts generated by STAR were analyzed by using DESeq2 package (Love et al., 2014) for detecting differentially expressed genes (DEGs). An adjusted *p-value* cut off of 0.05 was decided as threshold for detection of DEGs. Starting from the expression matrix, genes considered as differentially regulated were analyzed using hierarchical clustering method (cluster function, stats package). The enriched annotation table results, obtained in the web site, were then downloaded to be processed in R/bioconductor and visualized using ggplot2 package. The combined score is a combination of the logarithm of the *p-value* computed using the Fisher's exact test and the rank score computed using a modification to Fisher's exact test, in which it was computed a z-score for deviation from an expected rank. Visualization of the clustering and heatmap of log2-normalized counts (TMM method) were obtained using gplots package. To explore the high-dimensional property of the data, the PCA (Principal Component Analysis), as dimensionality reduction algorithm implemented in stats package, was used. For th≤e Functional Annotation analyses, Enricher web tools were used.

p53 siRNA

SW837 cells were transfected with 100 nM of siRNA against p53 (SMARTpool p53) and negative nonspecific siRNA (Non-targeting Pool), for 72h, as reported (Soares et al., 2016), and then seeded at 2.25 × 10^5 cells/well, followed by MANIO treatment. Protein extracts were analyzed by western blot as described above.

Cellular thermal shift assay (CETSA)

CETSA experiments were performed as reported (Tan et al., 2015; Raimundo et al., 2018). In whole SW837 cells, treatments with MANIO were carried out for 4 h. Soluble protein was detected by western blot as described above.

Comet assay

The alkaline comet assay was used to evaluate DNA damage HCT116 $p53^{+/+}$ cells, as described (Raimundo et al., 2018). Tail DNA was quantified using Fiji Software (Open Comet/ImageJ) (Gyori et al., 2014; Schindelin et al., 2015).

Micronucleus test

The cytokinesis block micronucleus assay in human lymphocytes was performed as described (Soares et al., 2017).

Recombinant human wt and mutp53 R248W DBD protein production

Human wt and mutp53 R248W DBD were subcloned into the vector pETM-20 as described (Gomes et al., 2018), but with some modifications. *Escherichia coli* cells, expressing recombinant proteins, were harvested by centrifugation and chemically lysed in NZY Bacterial Cell Lysis Buffer (Nzytech, Lisboa, Portugal), 5mM dithiothreitol (DTT), and 10 μM $Zn(CH_3CO_2)_2$ following manufacturer's instructions. Samples were filtrated (0.2 μm), loaded onto a HiTrap Heparin HP column (GE Healthcare, VWR), and proteins eluted with a NaCl step gradient (0 - 0.3 M) at 1.5 mL/min. Further purification was achieved by gel filtration chromatography using a HiPrep 16/60 Sephacryl S-100 High-Resolution column (GE Healthcare, VWR) in a Fast Protein Liquid Chromatography (FPLC) system (Pharmacia Biotechnology, GE Healthcare, VWR). Running buffer contained 50 mM HEPES pH 7.5, 5 mM DTT, 10 μM Zn $(CH_3CO_2)_2$, and 150 mM NaCl. Pure protein fractions were analyzed using SDS-polyacrylamide gel electrophoresis, while protein concentration was measured spectrophotometrically.

Protein-ligand interaction by fluorescence quenching

Evaluation of the binding of MANIO to recombinant human wtp53 and mutp53 R248W DBD was based on the quenching of the proteins' intrinsic fluorescence. Phosphate buffer consisting of 50 mM HEPES, 5 mM DTT, 10 μM Zn $(CH_3CO_2)_2$, and 150 mM NaCl (pH 7.5) was used in the preparation of all solutions. Briefly, 5 μM of each protein, increasing concentrations of drug solution (0 – 75 μM) and phosphate buffer solution (pH 7.5) were mixed to a final volume of 280 μL. Fluorescence emission spectra were recorded at room temperature (23 ± 1°C) in a microplate reader (Synergy HT Multi-Detection Microplate Reader, BioTek®, Izasa Scientific) in the range of 300 – 350 nm upon excitation at 260 nm.

Proteins-MANIO binding parameters were calculated using the Origin 8.5.1 software v8.5.1 (OriginLab Corporation, Northampton, MA, USA). The fitting of the experimental values was made according to the Langmuir binding equation. The protein binding parameters of the interaction monitored by fluorescence were calculated through the fitting of the experimental points to the following equation (adapted from Fernandes et al., 2017):

$$[protein - MANIO] = \frac{I_0}{I} - 1 = \frac{y_{max}^{n}}{1 + \frac{K_d}{[MANIO]}}$$

where I_0 and I are the fluorescence intensities in the absence and presence of MANIO, respectively, y_{max} corresponds to the highest quenching induced by MANIO, *n* accounts for the number of binding sites, and K_d corresponds to the dissociation constant of protein-MANIO complexes.

In vivo antitumor and toxicity assays

Xenograft tumor assays were performed as described (Soares et al., 2017). Briefly, 1×10^6 (HCT116 $p53^{+/+}$ and $p53^{-/-}$) or 5×10^6 (SW837) cells were inoculated subcutaneously in mice dorsal flank. When tumors reached approximately 100 mm^3 volume, treatment started by intraperitoneal injections, twice a week with MANIO or vehicle (six animals/group), for two weeks. Tumor volumes, body weights or any signs of morbidity were regularly monitored until the end of the treatment. At the end of the study, animals were sacrificed by cervical dislocation and blood samples and organs (kidneys, spleen, heart, and liver) were collected for toxicological analysis.

Immunohistochemistry (IHC)

Preparation of tissues of HCT116 ($p53^{+/+}$ and $p53^{-/-}$) and SW837 tumors, staining with H&E or antibodies, assessment of TUNEL-positive cells, evaluation of 3,3′-diaminobenzidine (DAB) intensity, quantification of marked cells, and images acquisition were performed as described (Soares et al., 2017). Antibodies are listed in Key resources table.

Combination therapy assays

SW837 and patient-derived primary CCZ3 cells were treated with fixed concentrations of MANIO and increasing concentrations of doxorubicin (DOXO), cisplatin or 5-Fluorouracil (5-FU). The effect of combined treatments on cell proliferation was analyzed by SRB or MTT assays, for SW837 or CCZ3 cells, respectively, as described above. Combination index (CI) and dose reduction index (DRI) values were determined as described (Chou and Talalay, 1984; Raimundo et al., 2018).

Drug pharmacokinetic (PK) studies

In vitro (Eurofins, France) and *in vivo* (Pharmacology Discovery Services, Taiwan) PK assays were subcontracted.

In vitro PK assays

Description of *in vitro* PK assays.

Assay	Technique	Incubation	Detection method	Reference
Aqueous solubility (simulated gastric fluid)		24 h RT	HPLC-UV/VIS	(Lipinski et al., 2001)
Aqueous solubility (simulated intestinal fluid)		24 h RT	HPLC-UV/VIS	(Lipinski et al., 2001)
Aqueous solubility (PBS, pH 7.4)		24 h RT	HPLC-UV/VIS	(Lipinski et al., 2001)
Partition coefficient (LogD, n-octanol/PBS, pH 7.4)	Shake-flask	60 min RT	HPLC-MS/MS	(Sangster, 1997)
Protein binding (plasma, human)	Equilibrium dialysis	4 h 37°C	HPLC-MS/MS	(Banker et al., 2003)
A-B permeability (Caco-2, pH 6.5/7.4)		0 and 60 min RT	HPLC-MS/MS	(Hidalgo et al., 1989)
B-A permeability (Caco-2, pH 6.5/7.4)		0 and 40 min RT	HPLC-MS/MS	(Hidalgo et al., 1989)
Intrinsic clearance (human liver microsomes – 0.1 mg/mL)		0, 15, 30, 45, 60min RT	HPLC-MS/MS	(Obach et al., 1997)

A – Apical; B – Basal; HPLC-UV/VIS – High performance liquid chromatography – UV/Visible detector; HPLC-MS/MS – High Performance Liquid Chromatography Mass Spectrometry; RT – Room Temperature.

Aqueous solubility (μM) was determined by comparing the peak area of the principal peak in a calibration standard (200 μM) containing organic solvent (methanol/water, 60/40, v/v) with the peak area of the corresponding peak in a buffer sample. In addition, chromatographic purity (%) was defined as the peak area of the principal peak relative to the total integrated peak area in the HPLC chromatogram of the calibration standard.

The total amount of compound was determined as the peak area of the principal peak in a calibration standard (100 μM) containing organic solvent (methanol/water, 60/40, v/v). The amount of compound in buffer was determined as the combined, volume-corrected, and weighted areas of the corresponding peaks in the aqueous phases of three organic-aqueous samples of different composition. An automated weighting system was used to ensure the preferred use of raw data from those samples with well quantifiable peak signals. The amount of compound in organic was calculated by subtraction. Subsequently, LogD was calculated as the Log10 of the amount of compound in the organic phase divided by the amount of compound in the aqueous phase.

The peak areas of the test compound in the buffer and test samples were used to calculate percent binding and recovery according to the following formulas:

$$\text{Protein binding } (\%) = \frac{Area_p - Area_b}{Area_p} \times 100$$

$$\text{Recovery } (\%) = \frac{Area_p + Area_b}{Area_c} \times 100$$

where

$Area_p$ = Peak area of analyte in protein matrix
$Area_b$ = Peak area of analyte in buffer
$Area_c$ = Peak area of analyte in control sample

The apparent permeability coefficient (P_{app}) of the test compound was calculated as follows:

$$Papp\ (cm/s) = \frac{V_R \times C_{R,end}}{\Delta t} \times \frac{1}{A \times (C_{D,md} - C_{R,mid})}$$

where V_R is the volume of the receiver chamber. $C_{R,end}$ is the concentration of the test compound in the receiver chamber at the end time point, Δt is the incubation time, and A is the surface area of the cell monolayer. $C_{D,mid}$ is the calculated mid-point concentration of the test compound in the donor side, which is the mean value of the donor concentration at time 0 minute and the donor concentration at the end time point. $C_{R,mid}$ is the mid-point concentration of the test compound in the receiver side, which is one half of the receiver concentration at the end time point. Concentrations of the test compound were expressed as peak areas of the test compound.

The recovery of the test compound was calculated as follows:

$$Recovery\ (\%) = \frac{V_D \times C_{D,end} + C_{R,end}}{V_D \times C_{D0}} \times 100$$

where V_D and V_R are the volumes of the donor and receiver chambers, respectively. $C_{D,end}$ is the concentration of the test compound in the donor sample at the end time point. $C_{R,end}$ is the concentration of the test compound in the receiver sample at the end time point. C_{D0} is the concentration of the test compound in the donor sample at time zero. Concentrations of the test compound are expressed as peak areas of the test compound.

For permeability assays, lucifer yellow was used as the cell monolayer integrity marker. Lucifer yellow permeability assessment (in the Apical to Basal (A-B) direction at pH 7.4 on both sides) was performed after the permeability assay for the test compound. The cell monolayer that had a Lucifer yellow permeability of less than 1.5×10^{-6} cm/s for Caco-2 and MDR1-MDCKII cells and 2.5×10^{-6} cm/s for MDCKII cells was considered intact, and the permeability result of the test compound from intact cell monolayer is reported.

For intrinsic clearance determinations, metabolic stability, expressed as percent of the parent compound remaining, was calculated by comparing the peak area of the compound at the time point relative to that at time-0. The half-life ($T_{1/2}$) was estimated from the slope of the initial linear range of the logarithmic curve of compound remaining (%) versus time, assuming the first-order kinetics. The apparent intrinsic clearance (CL_{int}, in μL/min/pmol, μL/min/mg or μL/min/Mcell) was calculated according to the following formula:

$$CL_{int} = \frac{0.693}{T_{1/2} \times (mg\ protein/\mu L\ or\ million\ cells/\mu L\ or\ pmol\ CYP\ isoyme/\mu L)}.$$

In vivo PK assays

Animals

Male ICR mice weighing 25 ± 5 g were provided by BioLasco Taiwan (under Charles River Laboratories Licensee). Animals were acclimated for 3 days prior to use and were confirmed with good health. All animals were maintained in a hygienic environment with controlled temperature (20 - 24°C), humidity (30% - 70%) and 12 hours light/dark cycles. Free access to sterilized standard lab diet [MFG (Oriental Yeast Co., Ltd., Japan)] and autoclaved tap water were granted. All aspects of this work, including housing, experimentation, and disposal of animals were performed in general accordance with the Guide for the Care and Use of Laboratory Animals: Eighth Edition in our AAALAC-accredited laboratory animal facility. The animal care and use protocol was reviewed and approved by the IACUC at Pharmacology Discovery Services Taiwan, Ltd.

Animal dosing design - *in vivo* PK, non-fasted animals

Vehicle	Dose Schedule	Route	Dose		Mice (Male ICR)
			mL/kg	mg/kg	
DMSO/ Solutol® HS15/ PBS (5/10/85, v/v/v)	Bolus	IV	5	20	24[a] + 3[b]

[a]Plasma with 3 mice per time point; [b]Normal (untreated) blank control for drug free plasma.

MANIO formulation

MANIO was dissolved in dimethyl sulfoxide (DMSO)/ Solutol® HS15/ PBS (5/10/85, v/v/v) at 4 mg/mL for IV injection. The dosing volume was 5 mL/kg for IV.

Plasma sample collection from mice

Blood aliquots (300-400 μL) were collected via cardiac puncture in tubes coated with lithium heparin, mixed gently, then kept on ice and centrifuged at 2,500 × g for 15 minutes at 4°C, within 1 h of collection. The plasma was then harvested and kept frozen at −70°C until further processing.

Quantitative bioanalysis (plasma)

The plasma samples were processed using acetonitrile (ACN) precipitation and analyzed by LC-MS/MS. A plasma calibration curve was generated. Aliquots of drug-free plasma were spiked with the test substance at the specified concentration levels. The spiked plasma samples were processed together with the unknown plasma samples using the same procedure. The processed plasma samples were stored at −70°C until receiving LC-MS/MS analysis, at which time peak areas were recorded, and the concentrations of the test substance in the unknown plasma samples were determined using the respective calibration curve. The reportable linear range of the assay was determined, along with the lower limit of quantitation (LLOQ).

Pharmacokinetics

Plots of plasma concentration of MANIO versus time were constructed. The fundamental pharmacokinetic parameters of each compound after IV ($t_{1/2}$, C_0, AUClast, AUCInf, AUCExtr, MRT, Vss, and CL) was obtained from the non-compartmental analysis (NCA) of the plasma data using WinNonlin. Plots of plasma concentrations of compounds versus dose were constructed.

Modeling

The starting structure for the modeling was the crystal of wtp53 DBD tetramer bound to a DNA target (2AC0) (Kitayner et al., 2006), as described in a previous work (#94) (Gomes et al., 2020). The R248W mutation was performed using Chimera swapaa tool and then geometry optimized with the Amber18/ parm99SB (#100)(Hornak et al., 2006).

Molecular docking

Molecular docking of MANIO was performed using the AutoDock 4.2 suite of programs with the Lamarckian genetic algorithm (LGA) (#99) (Morris et al., 1998). A grid box was centered on residue 280 of chain A. The population was 300, the maximum number of generations was 27,000 and the maximum number of energy evaluations was 2,500,000.

Molecular dynamics (MD) simulations

MD simulations were performed using the Amber 18 molecular dynamics program with the parm99SB (Hornak et al., 2006) and GAFF force fields (Wang et al., 2004) for the complexes of DNA:wtp53 and DNA:R248Wp53 with the ligand MANIO. The structures were placed within an octahedral box of TIP3P waters (the distance between the protein surface and the box was set to 10Å) and counter ions were added to make the entire system neutral. The systems were subjected to two initial energy minimizations (with the steepest descent and conjugate gradient algorithms) and to 500 ps of equilibration in a NVT ensemble using Langevin dynamics with small restraints on the protein (10 kcal/mol) to heat the system from 0 to 300 K. Production simulations were carried out at 300 K in the NPT ensemble using Langevin dynamics with a collision frequency of 1.0 ps−1. Constant pressure periodic boundary conditions were imposed with an average pressure of 1 atm. Isotropic position scaling was used to maintain pressure with a relaxation time of 2 ps. The time step was set to 2 fs. SHAKE constraints were applied to all bonds involving hydrogen atoms (Miyamoto and Kollman, 1992). The particle mesh Ewald (PME) method (Darden et al., 1993)was used to calculate electrostatic interactions with a cut off distance of 10 Å. Two replicas of 50 ns simulations with different initial velocities were performed. The total combined time of the simulations was 200 ns. Cluster analysis was conducted with the DBScan clustering algorithm, with a minimum of 25 points and 1.5 Å as cut-off distance to form a cluster representation. The trajectories of the corresponding atoms were extracted and analyzed for the 100 ns using 6666 frames for each structure.

QUANTIFICATION AND STATISTICAL ANALYSIS

Statistical significance was calculated for each dataset based on at least three independent experiments. Data were analyzed using GraphPad Prism software v7.0 (San Diego, CA, USA) and are presented as means ± SEM. Appropriate statistical tests were applied to each dataset ; $p < 0.05$ was considered statistically significant.